NTNU

Norwegian University of
Science and Technology

Partial Discharges and Breakdown Voltage in Designs with Triple Junctions under AC Stress.

Kristine Korneliussen

Master of Energy and Environmental Engineering
Submission date: June 2016
Supervisor: Frank Mauseth, ELKRAFT
Co-supervisor: Atle Pedersen, SINTEF Energy Research

Norwegian University of Science and Technology
Department of Electric Power Engineering

Problem Description

Due to environmental issues, it is a trend today to avoid climate gasses like SF_6. Thus, the use of air as insulation gas has lately been highly in focus for producers of high voltage equipment. The withstand voltage of air is lower than SF_6, and the challenge for electrical engineers is to make compact air insulated equipment. It is common to use barriers in the design to increase the path of the streamer and thus increasing the withstand voltage.

During the design process it is common to use Finite Element Analysis to calculate the electrostatic field strength of the different components in the equipment. However, knowing the electrostatic field distribution is not sufficient to predict the withstand voltage. It is also necessary to model the discharge processes including inception and propagation of streamers. Therefore, we have started research efforts aimed at elaboration of numerical procedures for the computation of streamer behaviour.

The main topic of the work will be the study of partial discharges and breakdown voltage in designs with triple junctions under AC stress. Inception and propagation of streamers under AC and lightning impulse is important.The work will consist of both laboratory measurements and electrostatic field simulations. The experimental work consist of measurements of breakdown voltage and partial discharge activities, using optical measurements. Comparison of the results will be used to make design criteria for predicting the withstand voltage of more complex designs where triple junctions are common.

Preface

This work investigates the breakdown voltage and optical detection of partial discharges, for test objects containing triple junctions, during AC stress in ambient air.

I would like to thank my supervisor Frank Mauseth at NTNU, and co supervisor, Atle Pedersen at SINTEF Energy Resarch, for their guidance, assistance and encouragement when my results did not correspond to what was expected. I would also like to thank Robert Marskar at SINTEF Energy Resarch for invaluable assistance during this spring, and always having an open office. I would also like to thank Mari Melkevik for voluntarily reading through my Master Thesis. Finally, I would like to thank my fellow students at our office "F452 Consulting" for all the good conversations and funny antics.

Kristine Korneliussen
Trondheim, June 2016

Abstract

Today, manufacturers of medium voltage equipment are searching for alternatives to sulfur hexafluoride (SF_6) as the insulating gas. The advantageous thermal and molecular properties make it suitable as an insulating gas, however, it is a strong green house gas. With the present climate challenges, one of the measures of reducing emission of climate gases is to phase out the use of SF_6-insulated medium voltage switchgears. An environmentally friendly alternative is air, which has a lower withstand voltage than SF_6. For backwards compatibility, the primary manufacturers in this development is optimization (to compensate for lower withstand) of current designs without increasing the dimensions.

This work have investigated the breakdown voltage and optical detected partial discharges activity during AC stress in ambient air. The measurements have been carried out for two cylindrically symmetric test objects, containing triple junctions. These measurements have been supplemented by electric field simulations carried out in COMSOL Multiphysics.

Various gap distances between the electrodes have been tested. Correlation between gap distance, breakdown voltage, partial discharge activity, and inception voltage have been determined.

The withstand voltage of the investigated test objects proved to have a higher value than the dimensioning withstand voltage for streamer propagation in a sphere-plane arrangement.

Characteristic pattern of the partial discharge activity, optically detected with a photomultiplier tube, align with the commonly observed phase-resolved pattern for gliding discharges along a surface of a solid dielectric in air.

Streamer inception criterion based on applying the background field for calculating resulted in a dimensioning criteria where the withstand voltage of the investigated test objects is lower than the dimensioning inception voltage from calculations of the streamer inception criteria.

Sammendrag

Produsenter av komponenter til koblingsanlegg på mellomspenningsnivå har i de seinere år rettet fokus på alternativer til sulfurheksaflurid (SF6) som isolerende gass. De termiske og molekylære egenskapene til gjør den svært egnet som isolerende gass, men det er en sterk drivhusgass. Et av tiltakene å redusere utslippet av klimagasser er å fase ut bruken av sf6-isolerte koblingsanlegg på mellomspenningsnivå.

Et miljøvennlig alternativ til SF6 er luft, men luft har en lave holdfasthet. For å kompensere for lavere holdfasthet er en av de viktigste fokusområdene for produsenter å optimalisere dagens design, uten å øke dimensjonene.

Denne oppgaven har fokusert på måling av overslagsspenning og optisk deteksjon av partielle utladninger i luft ved påtrykt AC-spenning. Målinger har blitt utført på to sylinder-symmetriske testobjekter som inneholder trippelpunkter. Målingene har blitt supplement av elektriske feltsimuleringer, utført i COMSOL Multiphysics. Gapsavstanden mellom elektrodene har blitt variert, og relasjonen mellom gapsavstand, partiell utladningsaktivitet, overslagsspenning, og tennspenning, har blitt nærmere undersøkt.

Holdespenningen til de undersøkte testobjektene viste seg å ha en høyere verdi enn den dimensjonerende holdespenning for streamerprogagering i et kule-plate-oppsett.

Den partielle utladningsaktiviteten viste mønstre som korrelerer med mønstre for glideutladninger langs overflaten til et fast dielektrisk materiale i luft.

Beregning av streamerinitiering, basert på anvendelse av bakgrunnsfeltet for beregning, resulterte i et kriterium der holdespenningen til de undersøkte testobjektene er lavere enn den dimensjonerende holdespenning fra beregninger av streamerinitiering

Contents

1 Introduction

Today, a large percentage of the gas insulated medium voltage switchgears apply sulfur hexafluoride (SF_6) as the insulating medium. SF_6 is an electronegative gas with a high dielectric strength. Besides this, thermal and molecular properties make the gas very suitable as an insulating gas in high and medium voltage equipment [1]. Therefore SF_6 enables compact designs, which is often preferable in wind turbines, industry and ring main units.

However, SF_6 is a strong green house gas, with a global warming potential (GWP) of 23900 in a time horizon of 100 years [2]. In politics, global warming potential is used as the metric to quantify emissions of various substances relative contribution to climate change. Global warming potential integrates the Radioactive Forcing (RF), i.e. "the net change in the energy balance of Earth due to some imposed perturbation, of a substance over a given time horizon, relative to the RF of CO_2" [3]. One of the measures of reducing the emission of green house gases is to phase out the use of SF_6 insulated medium-voltage switchgears [4]. Therefore, manufacturers of medium voltage equipment are searching for alternatives to SF_6 as the insulating gas.

An environmentally friendly alternative to SF_6 is air. The withstand voltage of air is 5-10 times lower than of SF_6, and dimensions must be increased to obtain the same withstand. The primary manufacturers in development is working on optimization (to compensate for lower withstand) of current designs without increasing the dimensions.

One technique for compensating for the dimensions is increasing the gas pressure. However, this assumes the system to be placed inside pressurized tanks. Pressurized components reduce personal safety and increase the cost and risk of other equipment in event of failure.

Combining dielectrics of different properties within the same insulating system might cause undesired field concentrations and discharge activity. This is especially the case at the triple junction between solid insulator, air and conductor, when AC voltage is applied. When two different media, independent of the nature of the media (solid, liquid or gaseous), are put into contact, chargers are transferred from one media to the other, and charge equilibrium takes place [5].

Normally, the impulse withstand voltage is the dimensioning criteria in type test

requirements for medium voltage equipment, and AC withstand voltage requirement is then normally automatically fulfilled. However, if a higher AC withstand voltage is required in the type test, seen in the manufactures marked outside Europe, this might be the dimensioning criteria.

This work investigates partial discharges and breakdown voltage in designs with triple junctions under AC stress. The experimental work consists of measurements of breakdown voltage and optically detection of partial discharges. In addition, measurements are supplemented by electric field simulations carried out in COMSOL Multiphysics.

2 Theory

2.1 Townsend Mechanism

When an electron is subjected to an electric field, the electron will, due to the Coulomb force $F = q \cdot E$, move in the opposite direction of the electric field. Electrons lose a fraction, or all, of its kinetic energy each time it collides with a particle, meaning the elastic cross-section decreases with increasing electron energy [1]. At a given temperature, the energy accumulated by an electron between two collisions is, on average, proportional to the field strength and the mean free path length. The mean free path length is inversely proportional to the pressure. Townsend's first ionization coefficient α, gives the probability that one electron gives one ionizing collision per unit length in the field direction and can be given by;

$$N_e(x) = N_{ec} \cdot e^{\alpha x}, \tag{1}$$

where $N_e(x)$ is the number of free electrons at a distance x from the cathode per second, and N_{ec} is the number of electrons released from the cathode per second [1].

N_{ec} is a sum of two parts: First, independent of the conditions in the circuit and the gas, a certain number of electrons N_0 is generated per unit time. For Townsend discharges to occur, this is a necessary precondition. Second, electrons are released from the cathode due to bombardment by ions and photons. The probability that one electron is relased from the cathode for each positive generated ion is given by Townsend's second ionization coefficient γ [1].

At a given temperature, Townsend's theory predicts that breakdown is determined only by the electric field strength E, the air pressure p, and the gap distance d [1].

2.2 Streamer mechanism

There is observed that the electron avalanche becomes unstable if the avalanche exceeds a critical length l_c, i.e. N_{ec} exceeds a critical limit. Space charges will then influence the electric field.

Experimental results show that when the gap distance, the electric field strength,

or the pressure increases, Townsend breakdown criteria is no longer valid. Breakdown is then explained by streamer mechanism [1]. This applies to both homogeneous and inhomogeneous fields.

In gases with high a density of ions, breakdown may develop from a single avalanche. A large number of atoms or molecules are excited in the gas such that photons are emitted. Through photoionization, these photons can produce seed electrons in front of the streamer, and lead to subsequent avalanches. If the positive ions left behind the subsequent avalanches are located close enough, space charges in the main avalanche are extended and intensified, and a self-propagating streamer head is formed [1].

2.2.1 Streamer Inception

If a sufficient number for electrons N_c are generated due to the described ionisation, and a self-propagating streamer head is formed, a high conducting plasma develops between the electrodes [6, 7]. The streamer inception criterion is defined as;

$$\int_l \alpha_{eff}(E)dx = \ln(N_c), \tag{2}$$

where $\alpha_{eff}(E)$ is the electric field dependent effective ionization coefficient, including ionization, electron attachment, and detachment, l is the integration path along the field line, and $\ln(N_c)$ is a dimensionless parameter. Empirical data show typical values of $\ln(N_c) \approx 9 - 18$, dependent of the inhomogeneity of the field [6, 7]. The integration path starts at the point with maximum field and follows the field line provided that $\alpha_{eff}(E) > 0$. The integration path ends at the inception field, i.e. where $\alpha_{eff}(E) = 0$. For synthetic air, $\alpha_{eff}(E)$ is as given in Appendix A.1.

Figure 1 shows the withstand voltage U_w, as a function of the electrode distance d, for a sphere-plane arrangement. The graph is divided into three stages of streamer development: 1) Streamer inception, 2) Streamer propagation, and 3) Leader propagation. The last stage will not be described any further since this stage only are relevant for gap distances over one meter [6].

In the first stage of streamer development, the field distribution is weakly nonuniform. Curve 1 in Figure 1 illustrates the correlation between inception voltage U_i and the distance d between the electrodes. In this stage, the curve for the withstand voltage follows the inception voltage curve, implicating that breakdown is directly formed by inception. Therefore, between origin and point

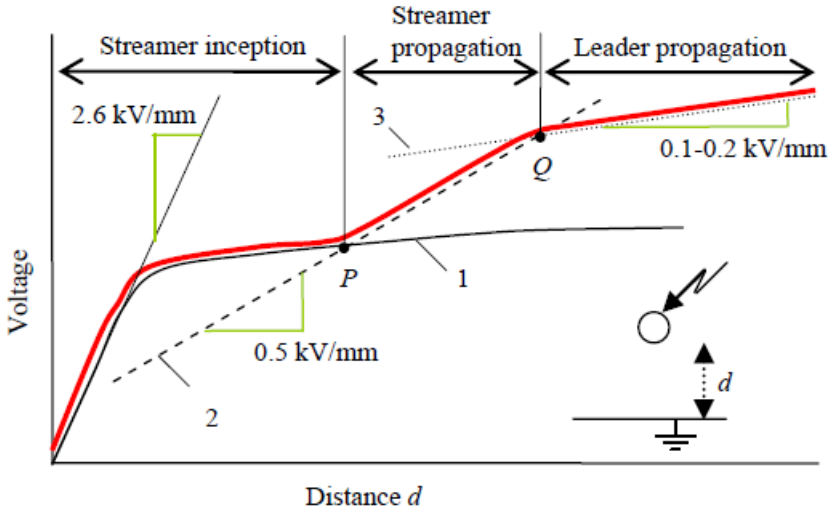

Figure 1: The figure shows the three stages of discharge development: 1) Streamer inception, 2) Streamer propagation, and 3) Leader propagation. The red curve illustrates the withstand voltage as a function of the electrode distance d for an inhomogeneous field arrangement (in this case a sphere-plane arrangement). Curve 1 presents the relationship between the inception voltage U_i and the distances between the electrodes. Curve 2 shows the lowest voltage that enables the streamer to short the electrodes in an inhomogeneous field [6].

P, the withstand voltage is determined and limited by the inception voltage. Based on eq. (2) and the numerical field calculations, U_i, and consequently the U_w, can be determined iteratively.

2.2.2 Streamer Propagation

In stage two, beyond point P in Figure 1, the field is strongly inhomogeneous, and the gap distance between the electrodes is increasing. In this stage, the streamer head will propagate towards the opposite electrode. However, the streamer will not short the electrodes immediately when the inception voltage is reached. The streamer head will only reach the opposite electrode if the propagation process is maintained over the entire gap length. Consequently, the applied voltage must be above a critical value $\geq U_i$. To satisfy a local criterion for the field in front of the streamer head, a sufficiently high potential difference between streamer head and opposite electrode is required. For gap distances above 40-50 mm an approximate value for the lowest voltage that enables the streamer to short the electrodes in an inhomogeneous field, can be expressed as the dashed curve shown in Figure 1:

$$U_w = U_0 + d \cdot E_{st}, \tag{3}$$

where d is the distance between the electrodes, E_{st} is the internal field strength along the positive streamer behind its head, and U_0 is the potential needed for the streamer head to generate a breakdown. Typical values are [6]: $E_{st} \approx 0.5(\pm 10 - 20)\%$ kV/mm (AC: 0.45 kV/mm, Impulse: 0.54 kV/mm) for positive streamer and $U_0 \approx 20 - 30$ kV. Negative streamers require a higher internal field strength in order to maintain a stable streamer propagation. Discharges from the negative electrode are therefore less critical than discharges from the positive electrode [6].

2.3 Partial Discharges and Phase-resolved Characteristic

In inhomogeneous fields, a self-sustained propagating discharge, called partial discharge, may not immediately lead to flash over, and the avalanche might only extend over the part of the gap where the electric field is sufficiently high. Phase-resolution of the discharge pattern may lead to clues about the nature of the discharge. Characteristic discharge patters versus power cycle of 50 Hz can be visualized on e.g. an oscilloscope [8, 9]. Typical patterns for discharges in ambient air, corona, and surface discharges are illustrated in Figure 2.

2.3.1 Discharges in Ambient Air - Corona

Figure 2a presents characteristic phase-resolved patterns for discharges in ambient air (corona). Phenomena differ depending on if they are observed around the positive or the negative electrode, i.e. positive or negative corona.

For negative corona, Trichel pulses may be observed above a certain stress [1]. If the voltage is constant Trichel pulses have approximately constant peak values, repetition frequency and pulse shape [1]. Trichel pulses may be observed while there are no discharges in the positive half-cycle. Negative corona has a lower inception voltage than positive corona. With increasing voltage, the repetition frequency will have a continuously and rapidly increase until a transition to negative glow discharge occurs. The current in the gap then becomes stable, and continuous and luminous spot may be observed at the cathode. If the field is strongly inhomogeneous, discharges called feathers or negative streamers are observed in the transition region between glow discharge and breakdown [1].

In the case of positive corona, first, when increasing the voltage, there may be observed a series of discharges of short duration (Onset streamers) close to inception voltage. With further voltage increase, the discharge develops into a glow discharge which lead to a continuous, but varying, current. Next, in

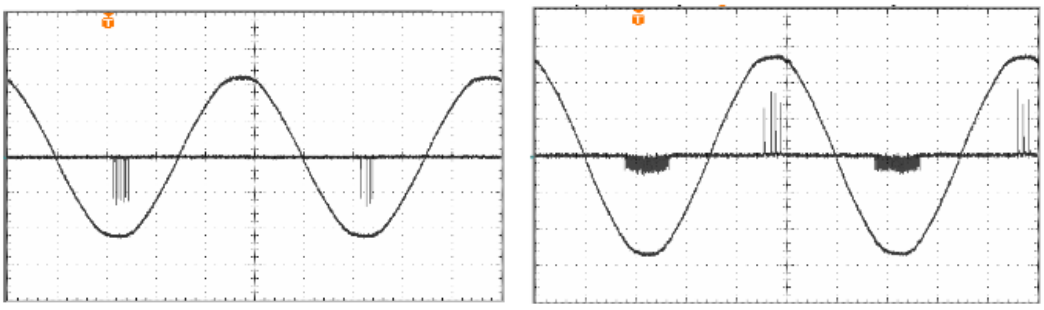

(a) Corona discharges in a needle plane gap in ambient air.

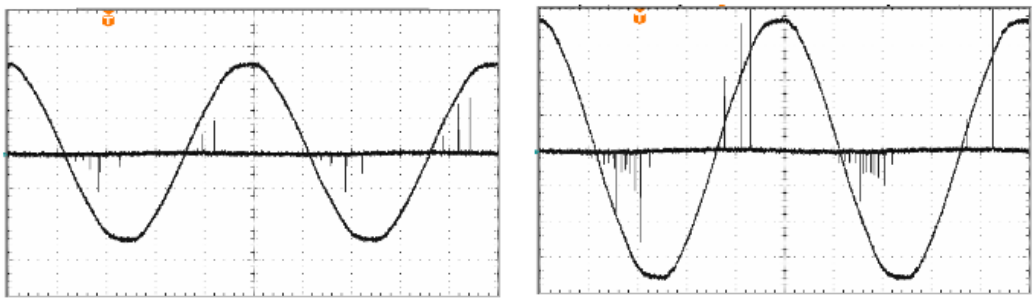

(b) Gliding discharges along a surface of a solid dielectric.

Figure 2: Phase-resolved partial discharge characteristics of different discharge models. Left side shows characteristics close to the inception voltage while right side show patterns substantially above the inception voltage [8].

addition to glow discharges, streamers or breakdown streamers are observed. If the voltage increase is maintained, streamers will reach the opposite electrode causing breakdown. A breakdown will usually develop in the positive half-cycle [1].

2.3.2 Discharges along Surfaces in Ambient Air

Characteristic phase-resolved patterns for discharges along surfaces in ambient air are displayed in Figure 2b. Surface discharges appear at the falling slope in the negative half-cycle and at the rising slope in the positive half-cycle. When voltage peaks are reached, pulse sequences suddenly disappear. When the inception voltage is exceeded, partial discharge activity is observed simultaneously in both positive and negative half-cycle. The magnitude of the pulses varies within a sequence even though the applied voltage is kept constant, and is dependent of the sign of the half-cycle. At rising test voltages, pulse magnitudes increase, whereas the pulse repetition rate changes only slightly [8].

2.3.3 Optical Method for Partial Discharge Detection

When partial discharges appear in electric insulation, different signals and forms of energy are emitted. Examples of emitted signals are; electrical, acoustic, and optical. There are several accepted techniques for measuring the various forms of signals.

Various ionization, excitation and recombination processes during partial discharges result in emitted radiation which may be detected optically. The optical method described further is based on using a photomultiplier for low light level detection of the emitted radiation.

All electric discharges emit radiation. However, the optical spectrum differs depending on the type of discharge. Chemical components in the insulation system influence the amount and wavelength of the emitted radiation. In addition, factors like pressure and temperature influence the absorption length. Therefore, the optical measured spectrum of a partial discharge depends on the intensity of the discharge and the surrounding insulation medium. The optical spectrum of partial discharges reaches from the ultraviolet to the infrared range [10].

In air, the spectrum of partial discharge is dominated by nitrogen emission. Partial discharges in air emit radiation from $280 - 410$ nm, with approximately $90 - 95\%$ of the radiation in the ultraviolet area. Most of the radiation from partial discharge is therefore invisible to the human eye. However, a small percentage of the emitted radiation, wavelengths above 400 nm, might be observable in complete darkness. A strong flash discharge contains wavelengths in the visible range of $400 - 700$ nm. In terms of surface discharges along a solid dielectric, the spectrum of the radiation is more complex and influenced by several factors, such as dielectric material, surface condition, chemical components in the surrounding gas, and electrode material [11].

2.4 Interfaces in Gas Insulated Systems

One of the weakest points in a high voltage insulation system is often the dielectric strength of the surface of a solid insulator used to separate the conductors [5, 12]. When materials of different nature are put into contact, a charge transfer occurs between the materials. Charge transfer might explain why metal-insulator interfaces constitute weak points in high voltage insulation systems. In gas insulated systems, contact contours between insulators, metallic

caps and the surrounding gas are denoted as triple junctions [5].

Field concentrations around triple junctions are in practice likewise to cause field distortions, facilitating breakdown. High field concentrations at the triple junction might set up a cathode mechanism which encourages the initiation of discharges. Streamers initiated might travel more rapidly across insulator surfaces in air compared to streamer propagation in air without an insulator. In addition, charges deposited on the surface by corona might alter the electric field distribution, encouraging breakdown [12].

2.5 Correction Factors for Atmospheric Conditions

The breakdown voltage U of a given air insulated configuration is dependent on the temperature T, the pressure p, and the humidity h. Thus, it is appropriate to apply correction factors for converting the breakdown voltage to a value that is referred to the standard reference atmospheric conditions T_0, P_0, and h_0 where: $T_0 = 20\,°\mathrm{C}$, $p_0 = 101.3\,\mathrm{kPa}$, and $h_0 = 11\,\mathrm{g\,m^{-3}}$ [12].

The breakdown voltage for a given path increases with increasing air density or humidity, provided that the relative humidity in air is below 80 %. The disruptive discharge voltage is proportional to the atmospheric correction factor k_t, where k_t is the product of the air density correction factor k_1, and the humidity correction factor k_2 [1].

$$U = k_t \cdot U_0 \tag{4}$$

$$k_t = k_1 \cdot k_2 \tag{5}$$

Air density correction factor k_1

The air density correction factor k_1 is expressed as:

$$k_1 = \delta^m, \tag{6}$$

where m is an exponent extracted from Figure 3, and δ is the relative air density given by,

$$\delta = \frac{p}{p_0} \cdot \frac{T_0}{T}, \tag{7}$$

where T and T_0 are expressed in Kelvin.

Humidity correction factor k_2

The humidity correction factor k_2 is given by

$$k_2 = k^w, \tag{8}$$

where w is an exponent extracted from Figure 3, and k a function depending on the type of test voltage, i.e. AC voltage, impulse voltage or DC voltage. For AC voltage, k is given by,

$$k = 1 + 0.012 \left(\frac{h}{\delta} - 11 \right), \tag{9}$$

where h is the humidity and may be written as [13]:

$$h = RH \cdot M_{H20} \cdot \frac{e(T)}{R \cdot (T + 273.15)}. \tag{10}$$

RH is the relative humidity, M_{H2O} is the molar mass of water, R is the universal gas constant, and $e(T)$ is the vapor pressure of water at a given temperature [13].

Extracting m and w

The parameter g is considered when finding m in eq. (6) and w in eq. (8), and is given by

$$g = \frac{U_B}{500 L \delta k}, \tag{11}$$

where U_B is the 50 % disruptive-discharge voltage expressed in kV, L is the minimum discharge path expressed in meters, and δ and k is the values derived from eq. (7) and eq. (9) [1].

When g is extracted, m and w are derived from Figure 3.

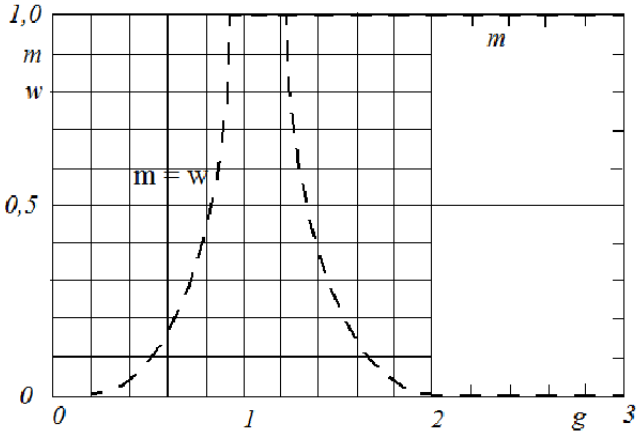

Figure 3: Exponent values m for air density correction and w for humidity conditions as a function of the parameter p [1].

3 Experimental Set-up and Measurement Method

The experimental set-up and measurement method are based on experiments measuring breakdown voltage under AC stress [14, 15].

3.1 Experimental Set-up

This section presents the measurement circuit and the test objects, followed by a description of the photomultiplier tube and the Series Mixed Signal Oscilloscope.

3.1.1 Measurement Circuit

Figure 4 shows the test circuit designed for investigating the breakdown voltage and optical detection of partial discharges during AC stress in ambient air.The rectangle in the upper part of Figure 4 illustrates the test cell, i.e. the area where high voltage is available. Optical partial discharge detection, carried out using a photomultiplier tube, requires this area to be blacked. Darkening is achieved by enclosing the test cell with black curtains.

The voltage supply to the test object is controlled using a variac connected to a step-up 220:100 kV transformer. The Root mean square value of the voltage supply is displayed on a multimeter connected to the variac. The test object is connected to the secondary side of the transformer through a water resistance. In order to reduce the short circuit currents, and thereby protect the transformer and the variac from these high currents at flash over, the resistance contains of demineralized water. A Hamamatsu R2055 photomultiplier tube, supplied by a DC source, is located in a distance approximately 5·gap distance from the test object. Channel one on the oscilloscope is connected to the photomultiplier tube (PMT) through a 50 Ω coaxial cable, and terminated with a 50 Ω resistance into the oscilloscope. Channel three is connected to the primary side on the transformer through an one phase transformer, designed for reference measurement. The signal on channel three is used as a reference for relating the signal on channel one to a phase angle.

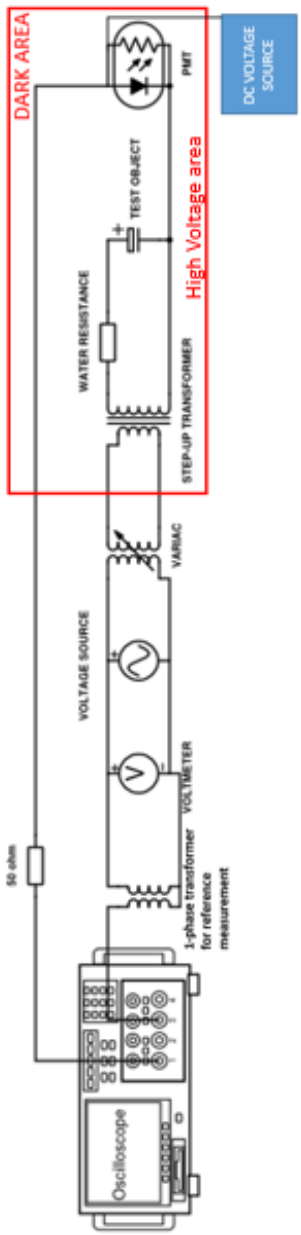

Figure 4: Principal sketch of the experimental set-up. The test object is supplied through a water resistance connected to the secondary side of a step-up transformer.Partial discharge activity is optically detected by the PMT. Optical detection of partial discharges requires the test cell, illustrated with the upper rectangle, to be blacked. The PMT is supplied by a DC voltage. Signals from the PMT and the variac are displayed on the oscilloscope.

The physical appearance of the test cell, i.e. the upper rectangle in Figure 4, is shown in Figure 5. The green rectangle encloses the demineralized water resistance, the orange rectangle encloses the step-up transformer, and the white area encloses the PMT. The test object is enclosed by the light blue rectangle.

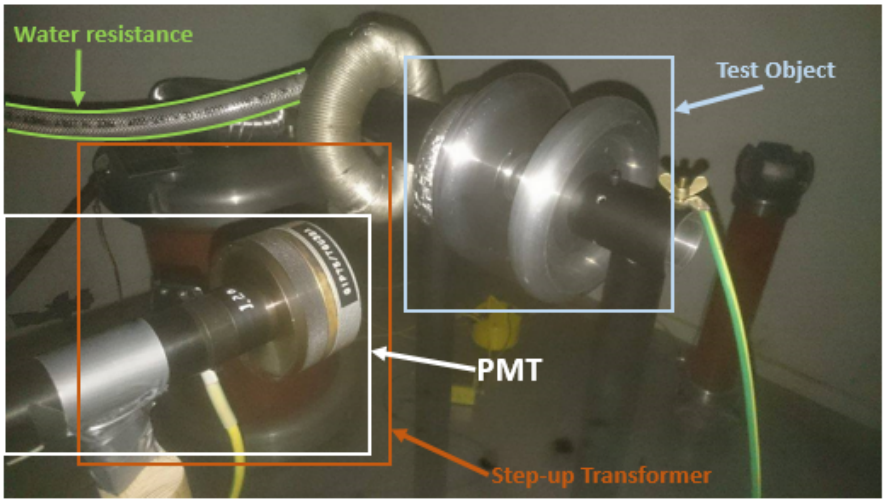

Figure 5: Dark/high voltage area, marked with the upper rectangle in Figure 4. The green rectangle encloses the demineralized water resistance, the orange rectangle encloses the step-up transformer, and the white area encloses the PMT. The test object is enclosed by the light blue rectangle.

3.1.2 Test Object

Two dimensional models of the investigated test objects are shown in Figure 6. The configurations consist of a combination of the three geometries presented in Figure 7. The electrode geometries are mounted on a cylindrical insulating rod. The basis geometry, displayed in Figure 7c, is used in order to avoid sharp edges and undesired partial discharges [9].

Config. 1, displayed in Figure 6a, has the geometry in Figure 7b on the high potential side and the geometry in Figure 7a on the grounded side. Config. 2, displayed in Figure 6b, has a geometry that includes the geometry in Figure 7a on both electrons.

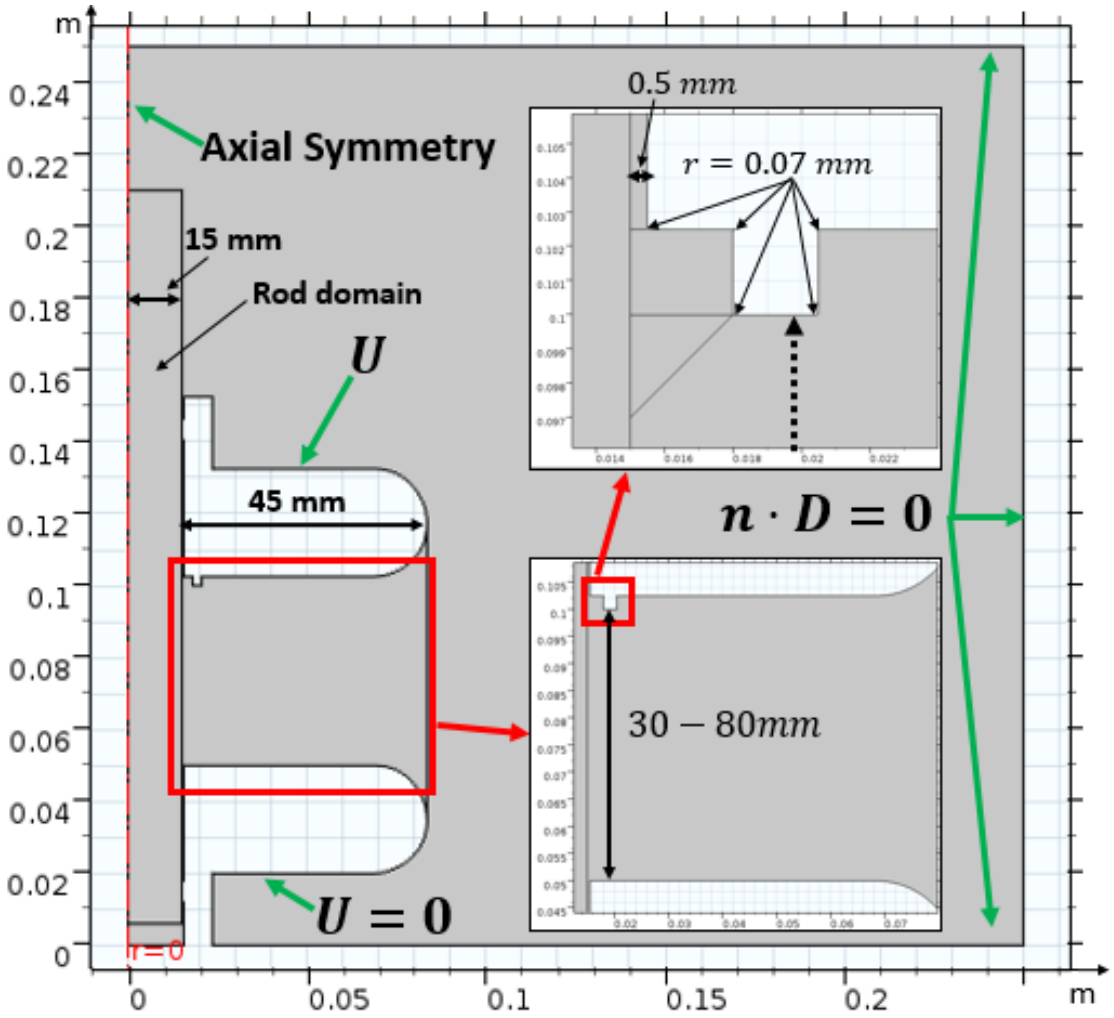

(a) Two dimensional model of Config. 1. The configuration has the geometry in Figure 7b on the high potential side and the geometry in Figure 7a on the grounded side. Pictures to the right display enlarged pictures of the gap between the electrodes.

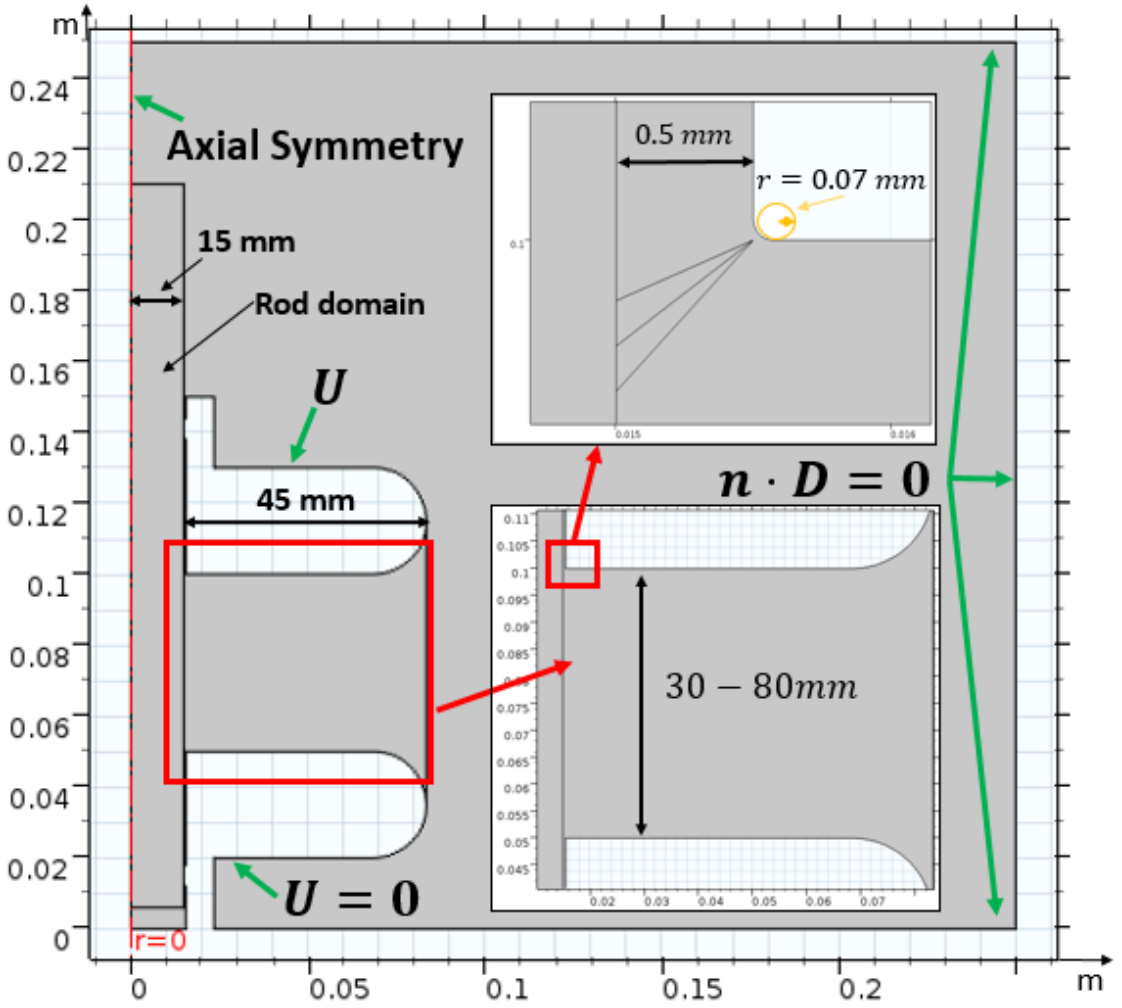

(b) Two dimensional model of Config. 2. The configuration has a geometry that includes the geometry in Figure 7a on both electrons, i.e. an cylindrical symmetry. Pictures to the right display enlarged pictures of the gap between the electrodes.

Figure 6: The investigated configurations include the geometry in Figure 7a on the grounded side. Config. 1, shown in 6a has the geometry in Figure 7b on the high voltage potential side. Config. 2, shown in 6b, consists of the geometry in Figure 7a on the high voltage side. The geometry in Figure 7c is seen as the region where $d = 45\,\text{mm}$.

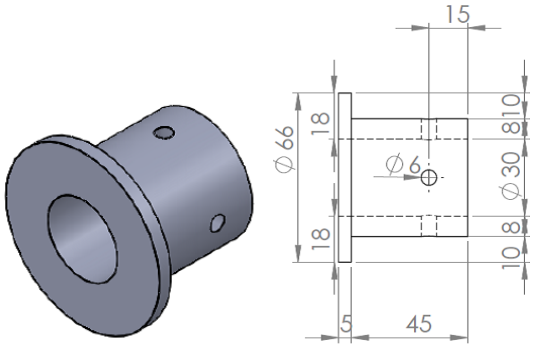

(a) "Flat" electrode geometry.

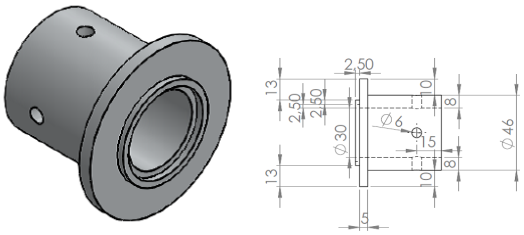

(b) "Sharp Edge". Has a 2.5 mm wide and long circular edge in a distance of 2.5 mm from the rod.

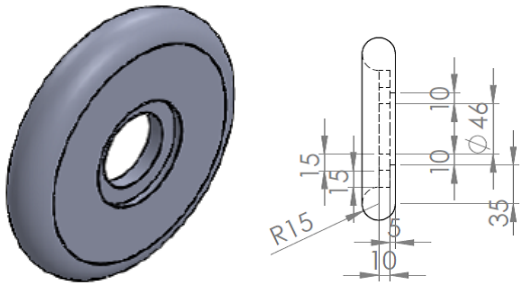

(c) "Basis" electrode. The basis geometry is used in order to avoid undesired partial discharges in the the experimental set up.

Figure 7: Electrode geometries [14]. The investigated configurations include the geometry in 7a on the grounded side. Config. 1 has the geometry in 7b on the high voltage potential side, whereas Config. 2 consists of the geometry in 7a on the high voltage side. The geometry in 7c is used in order to avoid undesired partial discharges.

3.1.3 Photomultiplier Tube (PMT)

Photomultiplier Tube (PMT) is a sensor well suited for low-light-level detection [17]. The PMT is a vacuum phototube consisting of an input window, a photocatode, several dynodes (focusing electrodes in vacuum that serves as an electron multiplier), and an anode (electron collector). The PMT detects certain ranges of the electromagnetic spectrum, typically ultraviolet, visible, and near-infrared wavelengths, and the detected light is converted into an electric signal, observable as a current pulse on an oscilloscope.

The operating principle is based on the external photoelectric effect [17]: When light strikes a metal or semiconductor placed in a vacuum, photoelectrons are emitted from its surface into the vacuum. Photoelectrons are then directed towards the first dynode in the multiplier tube and secondary electrons are emitted. The secondary electrons strikes the next dynode and additional secondary electrons are emitted. This process is repeated over the number of dynodes in the PMT. The secondary emitted photoelectrons are in the end collected by the anode and an amplified current is given as the output signal [18].

The amplified output current contains a small amount of current that is flowing in the tube even when operated in a complete darkness [18, 17]. This current is named "dark current" . The dark current creates noise on the output signal, and should therefore be kept as small as possible.

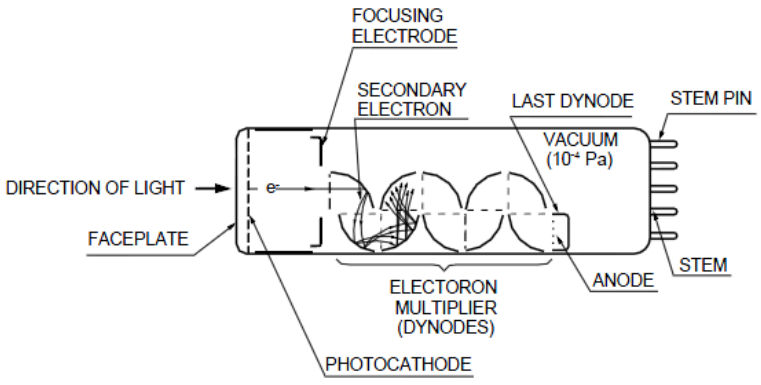

Figure 8: Cross section of head-On Type PMT [17, 18]

The photomultiplier tube used in this work is a Hamamatsu R2055, head-on type, 8 dynodes linear-forced tube. The cross section of the tube is shown in Figure 8. The main feature of the linear-forced tubes are fast time response, as well as good time resolution and pulse linearity [19]. The tube has a biakali (Sb-Rb-Cs, Sb-K-CS) photocatode with quartz as the window material in front of the photocathode. The spectal response of this type of PMT is in the ultraviolet to visible range, i.e. 180 nm − 650 nm. The wavelength of maximum response is 420 ± 30 nm. The maximum supply voltage between anode and cathode is $1500\,\mathrm{V}_{DC}$. The anode pulse output signal has a rise time of 0.8 ns [19].

3.1.4 Mixed Signal Oscilloscope

YOKOGAWA DLM2000 Series Mixed Signal Oscilloscope comes with a feature of acquisition and storage of the input signals [16].

When the waveform acquisition is executed, waveform data are stored in the acquisition memory. Based on the stored data, various operations can be performed [16].

One of the features is saving waveform data points as an ASCII (.csv extention) file. When waveform acquisition is stopped, past waveforms can be displayed using the history feature, .csv files can then be extracted [16]. In addition, the oscilloscope provides saving of screen shots on the format .png, using the screen shot feature. If acquisition is executed again, the accumulation is restarted, and the the past waveforms are deleted.

3.2 Measurement Method

The starting point for defining the measurement method is shown in Table 1. The table shows the requirements for 12 kV and 24 kV switchgear, general for equipment at these voltage levels.

3.2.1 Preliminary measurement

An aluminium wire is attached to the electrode with high voltage potential to create a arrangement where corona, according to Section 2.3.1, will occur. AC stress is applied to the electrode where the aluminium wire is attached, and an oscilloscope screen shot is saved.

Table 1: Type test requirements for 12 kV and 24 kV switchgear (IEC 60 071), general for equipment at 12 kV or 24 kV.

Test	Voltage		Duration	Repetitions
	12 kV_{rms}	24 kV_{rms}		
AC	28 kV_{rms}	50 kV_{rms}	60 s	1
Lightning impulse	75 kV	125 kV	1.2μs rise time, 50μs tail (50 % of peak value after 50μs	15

3.2.2 Defining sequences

Each configuration, presented in Section 3.1.2, is tested in two sequences. The sequences are defined as following:

- Config. 1, seq. 1: Config. 1 tested for distances $30 - 80$ mm with 10 mm between each tested distance.
- Config. 1, seq. 2: Config. 1 tested for distances $30 - 50$ mm with 10 mm between each tested distance.
- Config. 2, seq. 1: Config. 2 tested for distances $30 - 80$ mm with 10 mm between each tested distance.
- Config. 2, seq. 2: Config. 2 tested for distances $30 - 50$ mm with 10 mm between each tested distance.

3.2.3 Measurement procedure

When an alternating voltage is applied to a test object, breakdown voltage will be dependent of the time for which the voltage is applied.The rate of the voltage increase must therefore be specified [12].

One test repetition is performed as following:

- Increase the 50 Hz voltage amplitude with a slope between 0.075 and 0.087 kV/s on the electrode with high voltage potential until breakdown occurs.
- Extract the desired data as presented below.

- At 28 kV and 50 kV, the voltage is held for one minute before continuing increasing the voltage.
- If, based on the background experiments [14, 15], the breakdown voltage is expected to be quite higher than 28 kV or 50 kV, increase the voltage with a slope between 0.075 and 0.0087 kV/s to the voltage levels shown in Table 2.
- For each configuration, sequence, and gap distance, perform fifteen repetitions.

Table 2: Transition level between "rapidly" and "slowly" voltage increase.

Gap distance [mm]	**Voltage** [kV_{rms}]
80	50
70	45
60	37
50	28
40	23
30	16

The gap distance is adjusted to the distances presented in Table 2. The rod and the electrodes are cleaned with isopropanol when adjusting the gap distance. The rod is replaced with a new and unused rod when the electrode configuration is changed or, a new sequence is started.

Extraction of data during measurements

- The value of the breakdown voltage is registered for further statistical analyses.
- The temperature, the pressure and the relative humidity are registered continuous during the measuring process for normalizing the breakdown voltages to standard reference atmospheric conditions.

3.3 Electric Field Simulations

For finite element simulation and calculation of the electric field distribution, COMSOL Multiphysics version 5.2 is used.

The simulated models, shown in Figure 6, are build using Two Dimentional Axisymmetric and built-in geometries in COMSOL Multiphysics. The

parameters are set on the basis of electrode dimensions and the test object as explained in Section 3.1.2. The distance between the electrodes is set to $d = 50$ mm. In order to perform simulations, COMSOL requires the 90 degree angles to be rounded. For the triple junction, shown in the upper right corner in Figure 6, $r = 0.07\,\text{mm}$. This is the smallest radius that enables mesh in the defined geometries.

Electric potential is defined at the upper electrode, the lower electrode is set to zero potential, and the outer edges are defined with zero charge. Materials are defined for the different domains: For the air domain $\epsilon_r = 1$, whereas for the the rod domain $\epsilon_r = 4.6$. The mesh sequence type is “User-Controlled mesh” calibrated for general physics predefined “Normal” and “Free Triangular” for all domains. The element size is set to "Extremely fine" for the domain between the electrodes. In order to achieve a satisfactory number of nodes around the triple junction boundaries, “distribution” mesh is defined along the upper electrode and the lines between the electrode and the rod. The models are simulated for Frequency Domain, 50 Hz.

3.4 Prosessing of Data

3.4.1 Extraction of Data Files from the Oscilloscope

Number of history waveforms that are extracted from the acquisition memory is individual for each of the repetitions, and depending on the visual estimated number of periods with partial discharge activity before breakdown. Example of one screen shot is shown in Figure 9.

The following processing has been carried out on the data saved in the acquisition memory on the oscilloscope:

- Waveform data points are saved as ASCII (.csv extention) files.
- Screen shots are saved as .png files by utilizing the screen shot feature.
- Number of breakdown developed from the potential electrode, the grounded electrode, and unknown location, are visual estimated from the screen shots.
- Number of periods with partial discharge activity before breakdown are visual estimated from the screen shots.

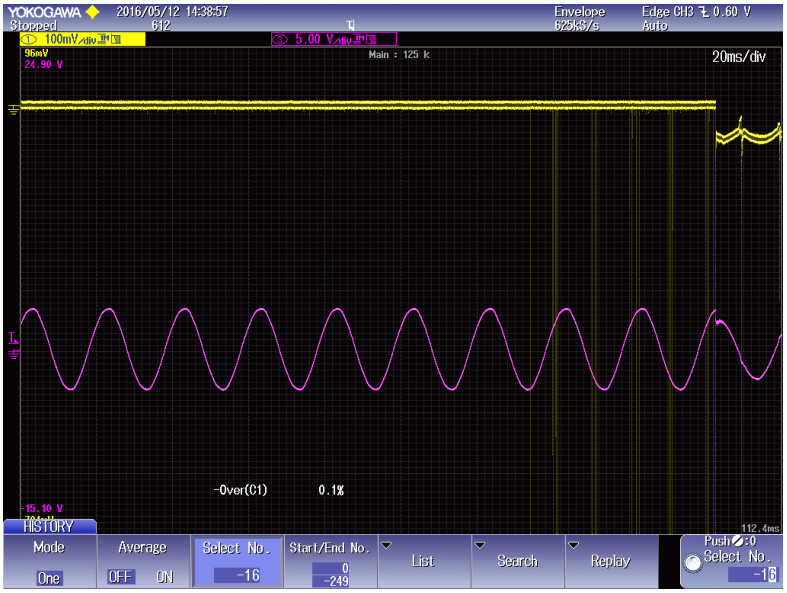

Figure 9: Example of screen image on oscilloscope. The upper signal (Channel one) is the signal from the PMT. The lower signal (Channel three) is the voltage extracted on the primary side of the transformer. This signal is displayed as a reference for interpretation of the signal on channel one.

3.4.2 Data from Measurements

Average breakdown voltage [kV_{peak}] with curve fitted linear polynomials, standard derivation, standard error (SE), and 99 % minimum confidence values, are calculated and plotted using build-in statistical functions in Excel.

3.4.3 Number of Partial Discharges as a Function of Phase Angle

.csv files, extracted from the acquisition memory on oscilloscope, are evaluated using the MATLAB script in Appendix A.3. The script reads data in .csv format and searches for values of partial discharges lower than certain noise limits presented in Table 5 in Appendix A.3. When all files are read, number of discharges are plotted as a function of the phase angle. A cosine curve is plotted in the same graph as a reference for the phase angle.

The limits for noise and break of loop are chosen on the basis of the screen shots extracted during the measurements, as well as "Trial and error" of the limit as a parameter in script.

4 Results and Discussion

This section presents the results obtained through implementation of the experimental method described in Section 3.2. All numerical values are normalized to standard atmosphere conditions by applying the equations given in Section 2.5.

The focus of this section will be on tendencies and correlations rather than exact values. Breakdown voltage and partial discharge activity are stochastic processes and will, by nature, be affected by random variations.

4.1 Breakdown Voltage

This section presents results from the measurements of the breakdown voltage. The measurements evaluated in this section are obtained from Config. 1, Seq. 2, and Config. 2, Seq. 2 defined in Section 3.2.2, i.e. measurements for gap distances of 30 to 50 mm.

The following results are presented:

- Average breakdown voltage U_{50}, standard error (SE), linear curve fitted polynomials, and 99 % minimum confidence values, presented in Figure 10.
- Number of measurements where breakdown is visually estimated to develop from the potential electrode, the grounded electrode, and unknown location, presented in Figure 11.

Figure 10 shows the average breakdown voltage U_{50} (vertical axis) as a function of the gap distance d (horizontal axis). Linear polynomials, derived by applying the method of least squares, 99 % minimum confidence values, and standard errors are extracted from the average breakdown voltages. The blue points and lines represent Config. 1, and the red points and lines represent Config. 2. In addition, the dimensioning withstand voltage for streamer propagation in a sphere-plane arrangement, described by eq. (3) in Section 2.2.2, is illustrated with the green dotted line for visual comparison. The average breakdown voltages as a function of the gap distances for Seq. 1 (measurements at gap distances $30 - 80$ mm) are shown in Figure 18 in Appendix A.2.

Comparing the dotted lines for both configurations with the green dotted line shows that for a gap distance of 30 mm, the withstand voltages for the investigated test objects are approximately equal the dimensioning withstand

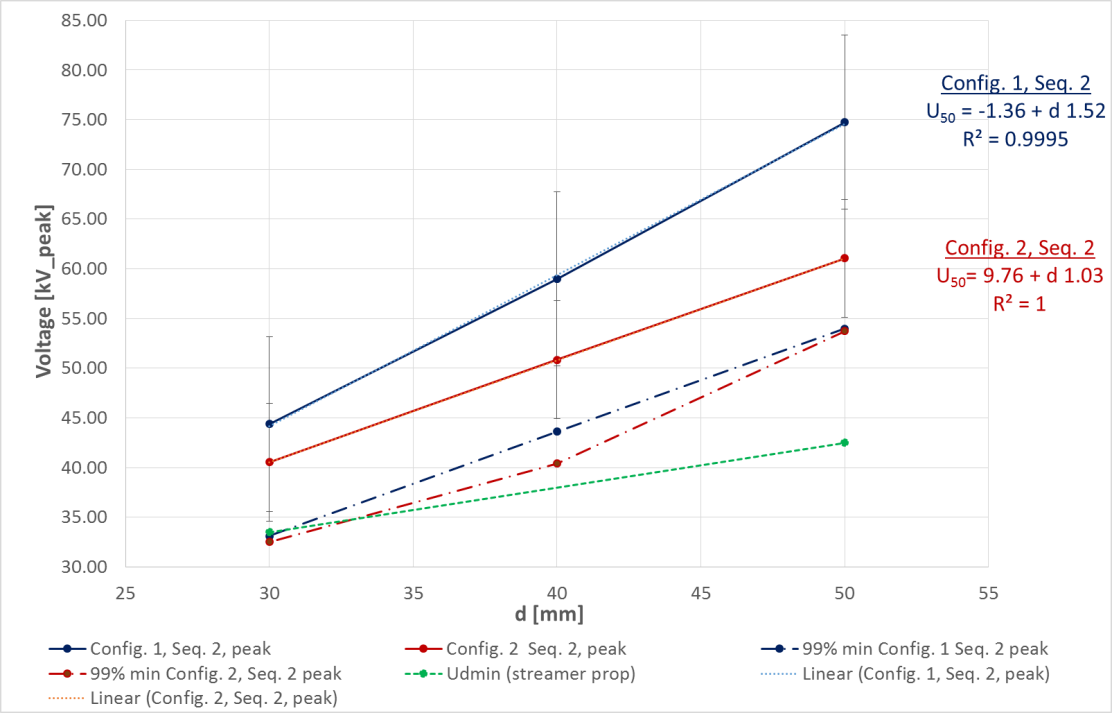

Figure 10: Average breakdown voltage U_{50} (vertical axis) as a function of gap distance d (horizontal axis); linear polynomials, standard error (SE), and 99 % minimum confidence values for Seq. 2. The blue points and lines represent Config. 1, and the red points and lines represent Config. 2. The green line illustrates eq. (3) with associated parameters for AC stress, i.e. the smallest predicted voltage that enables the streamer to short the electrodes in a sphere-plane arrangement.

voltage for streamer propagation in a sphere-plane arrangement. With increasing gap distance, the investigated test objects have a higher withstand voltage than the dimensioning withstand voltage in Section 2.2.2, and the deviation increases with increasing gap distance. This correlation is also observable in Figure 18 in Appendix A.2. Therefore, a prediction may be that the withstand voltages for the investigated test objects and gap distances are located in the area of streamer inception, i.e. to the left of point P in Figure 1.

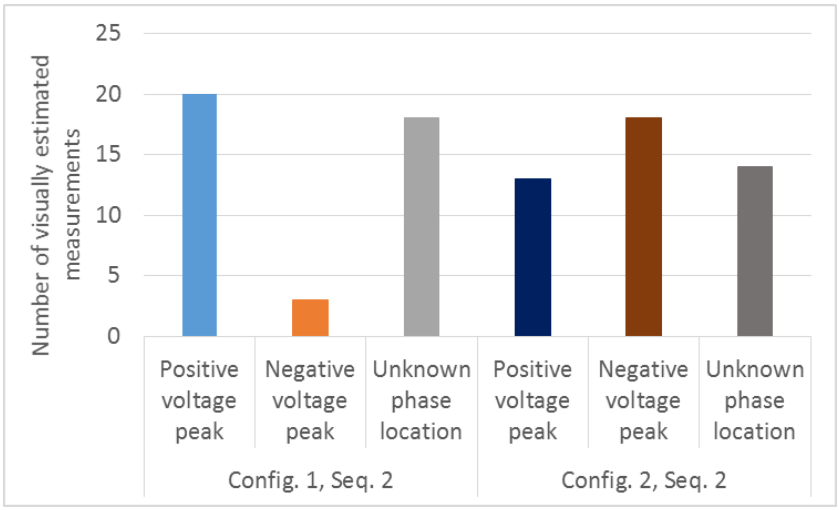

Figure 11: Number of measurements where breakdown is observed around positive voltage peak (developing from the potential electrode), negative voltage peak (developing from the grounded electrode), and unknown location presented as a function of the location on the phase location and the configurations.

Figure 11 shows the number of measurements (vertical axis) where breakdown is visually estimated around positive voltage peak, negative voltage peak and unknown phase location, presented as a function of the phase location and the configurations (horizontal axis). Positive voltage peak implies that breakdown is developed from the electrode where voltage is applied, i.e. the potential electrode in Figure 6. The numbers on the horizontal axis state that for Config. 1, the largest number of breakdown develop from the electrode with the sharp edge, i.e. the potential electrode. For Config. 2, breakdown may occur around either positive or negative peak with roughly equal probability. This is expected since Config. 2 consists of identical electrodes. Due to reflection symmetry, a positive streamer may develop at the grounded electrode at the negative voltage peak in the same way it does on the live electrode at the positive peak.

4.2 Partial Discharge Activity

This section presents results related to partial discharge activity optically detected by the PMT. Measurements evaluated in this section are obtained from Config. 1, Seq. 2 and Config. 2, Seq. 2.

Note that the signal magnitude from the PMT is not directly related to the magnitude [pC] of the partial discharge. In this work, the PMT is not calibrated for evaluating the correlation between the magnitude of the discharge and the observed pulse on the oscilloscope since this is considered to be outside the scope of this work.

There is an area on the rear of the rod which is optically screened so that the PMT can not detect optical activity in this area. Furthermore, results from the PMT do not tell where partial discharge activity is located along the test object, and they are therefore only an indication of activity or not.

The following results are presented in this section:

- Figure 12 shows a typical oscilloscope screen shot where corona is detected.
- Figure 13 shows a selected screen shot from the oscilloscope where partial discharge activity is optically detected.
- Figure 14 shows phase resolved number of discharges detected before breakdown.
- Figure 15 shows visually estimated number of periods with partial discharge activity before breakdown occurs, plotted versus the background field.

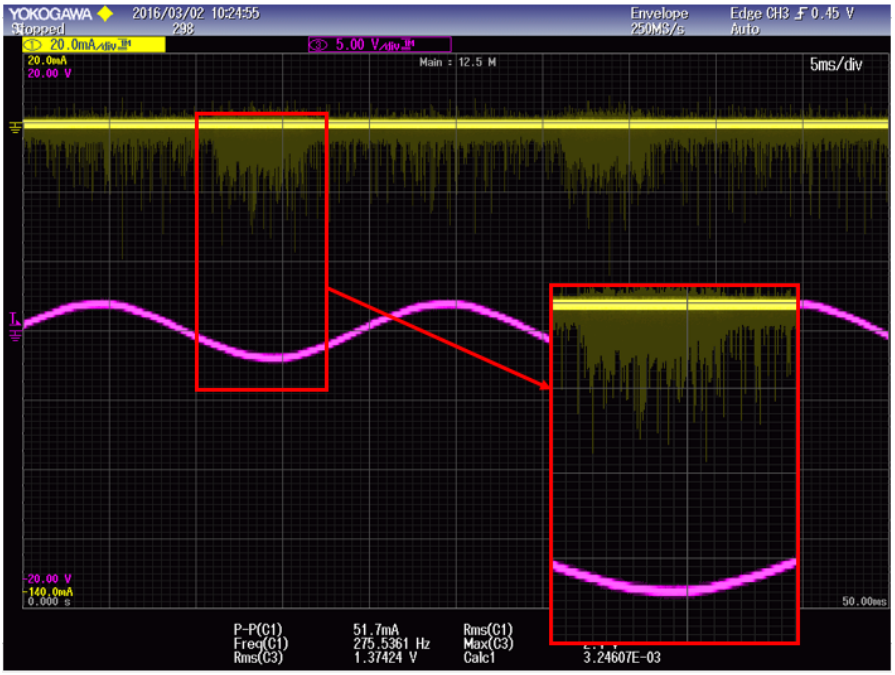

Figure 12: The upper oscilloscope signal shows optically detected partial discharge activity in the test area that corresponds with the characteristic patterns for discharges in ambient air, corona, shown in Figure 2a. Partial discharge activity is located around the voltage peaks, where most of the activity is located around the negative voltage peaks. The rectangle shows an enlarged image of a negative voltage peak where partial discharge activity is shown. The lower oscilloscope signal shows the voltage signal, shown as a reference for relating the upper oscilloscope signal to a phase angle.

Figure 12 shows a phase resolved screen shot with discharge activity. The upper oscilloscope signal shows optically detected partial discharge activity in the test area that corresponds with the characteristic phase resolved patterns for discharges in ambient air, corona, shown in Figure 2a. The discharge activity is located around the voltage peaks with most of the activity around the negative peaks. The rectangle shows an enlarged image of a negative voltage peak where partial discharge activity is visible.

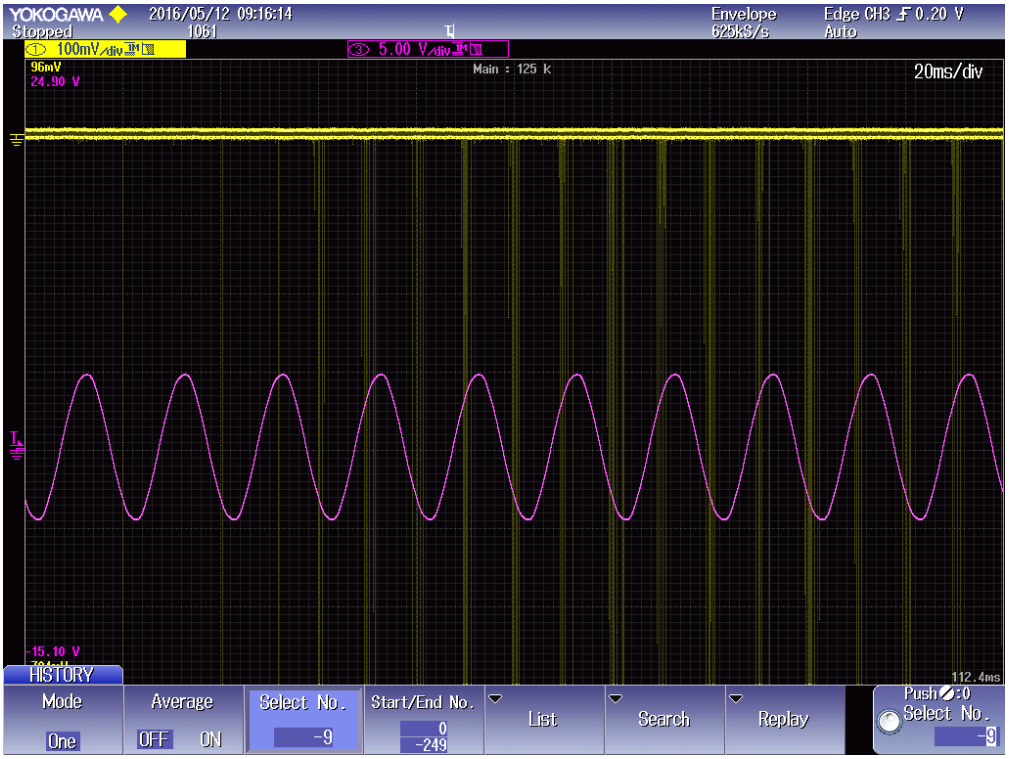

(a) Screen shot, 15-25 periods pre-breakdown. Partial discharge activity is observed starting in the second period of the screen image.

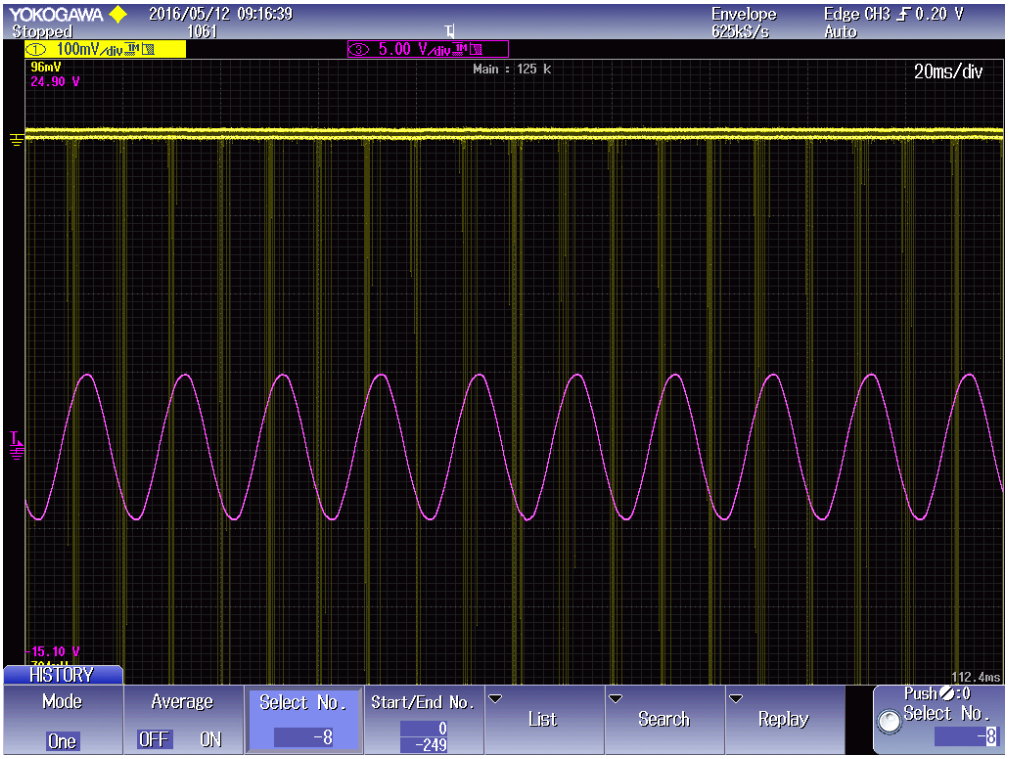

(b) Screen shot, 5-15 periods pre-breakdown. Partial discharge activity is observed for all the periods of the screen image.

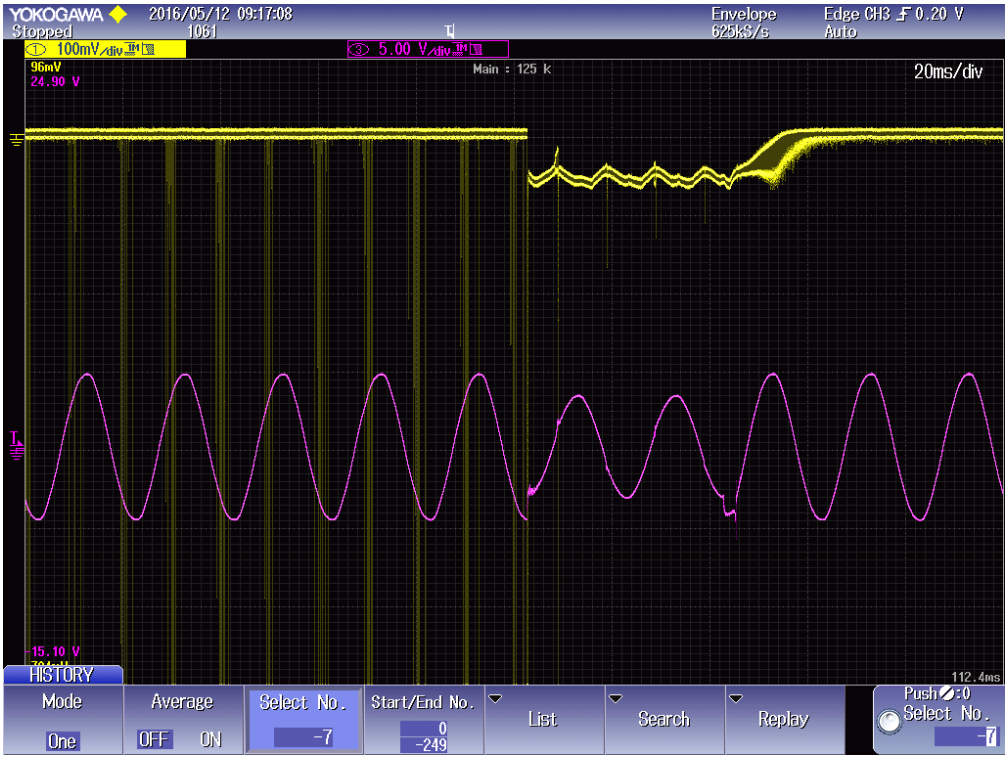

(c) Screen shot, 1-5 periods pre-breakdown and post- breakdown. Breakdown is observed at the negative voltage peak for the sixth period.

Figure 13: Screen shots from the oscilloscope for Config. 2. $U_{BD} = 59.4\,kV_{peak}$, $d = 50\,mm$. The upper oscilloscope signal shows optically detected partial discharge activity in the test area, whereas the lower oscilloscope signal shows the voltage signal from the variac, shown as a reference for relating the upper oscilloscope signal to a phase angle.

Figure 13 shows the recorded signal for the sixth lowest breakdown voltage $U_{BD} = 59.4\,kV_{peak}$, in Config. 2, for a gap distance of 50 mm. The subfigures present consecutive screen shots. Number of periods with partial discharge activity before breakdown is visually determined to a value of 22.5 periods. It is seen that the largest amount of discharges are observed at falling slope in the negative half-cycle and at rising slope in the positive half-cycle. These findings align with the commonly observed phase-resolved pattern, seen in Figure 2b), for gliding discharges along a surface of a solid dielectric in air. Section 2.4 states that charges deposited on the surface might alter the electric field distribution, encouraging breakdown. Deposited charges is predicted to influence the discharge activity in the consecutive period. Furthermore, the residual charges from ionisation of the air may influence the discharge activity and the time aspect of the applied voltage must therefore be taken into account.

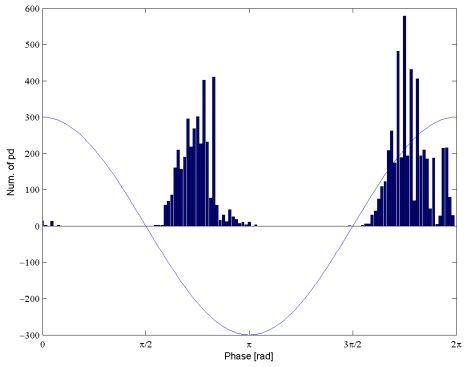

(a) Config. 1, Seq. 2, $d = 50\,\text{mm}$.

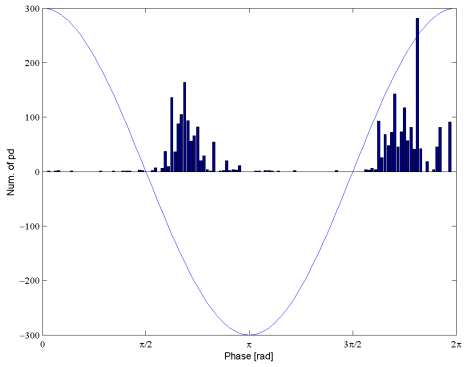

(b) Config. 2, Seq. 2, $d = 50\,\text{mm}$.

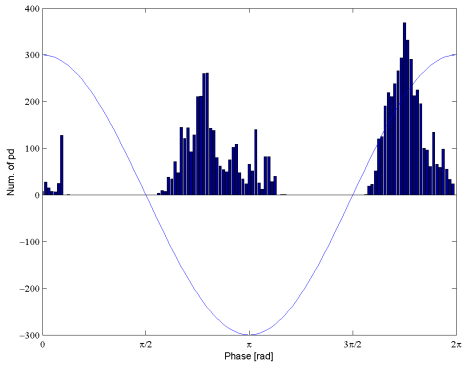

(c) Config. 1, Seq. 2, $d = 40\,\text{mm}$.

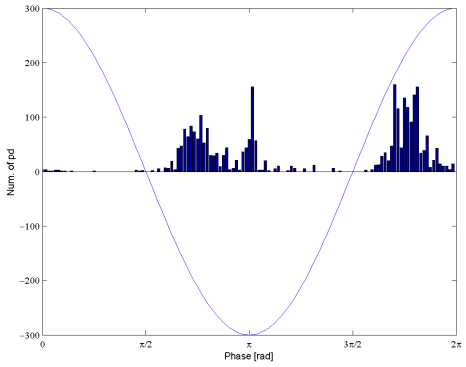

(d) Config. 2, Seq. 2, $d = 40\,\text{mm}$.

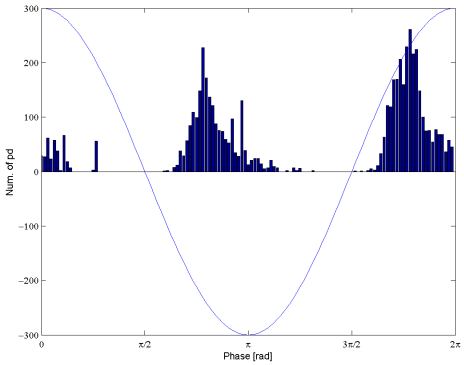

(e) Config. 1, Seq. 2, $d = 30\,\text{mm}$.

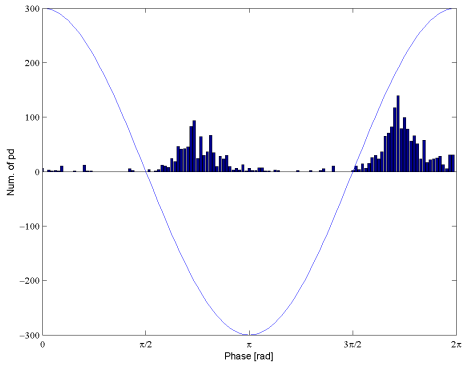

(f) Config. 2, Seq. 2, $d = 30\,\text{mm}$.

Figure 14: Number of discharges (vertical axis) observed before breakdown as a function of the phase angle (horizontal axis).

Figure 14 presents the number of discharges (vertical axis) observed before breakdown versus the phase angle (horizontal axis). Each subfigure is extracted by evaluating the .csv files for the specific parameters. The purpose of Figure 14 is to illustrate the phase-resolved distribution rather than the absolute number of partial discharges.

The subfigures in Figure 14 show that the largest amount of discharges are observed at the falling slope in the negative half-cycle and at the rising slope in the positive half-cycle. This applies for all investigated parameters and, as mentioned, the pattern align with the commonly observed phase-resolved characteristic for gliding discharges along a surface of a solid dielectric in air.

Figures 14a, 14c and 14e, plotted for Config. 1, have a larger number of optically detected partial discharges compared to Figures 14b, 14d and 14f, plotted for Config. 2. This is explained due to the fact that Config. 2 has a more homogeneous field distribution, and inception is predicted to immediately facilitate breakdown in homogeneous or weakly inhomogeneous fields.

Figure 15 shows the visually estimated number of periods with partial discharge activity before breakdown occurs . This figure shows that a gap distance of 50 mm, represented with the circles in the figure, has a smaller number of periods of activity before breakdown compared to the shorter distances, in the figure represented with the triangles and the diamonds. This may be a result of increased inhomogeneity with decreased gap distance.

Comparing Figures 15a and 15b shows that there in general, for equal value of the average background field, are fewer visually estimated periods with partial discharge activity before breakdown in Config. 2 compared to Config. 1. Higher partial discharge activity in Config. 1 can be explained by the inhomogeneity.

Figure 15b shows a tendency where smaller average background field results in increased number of periods with observed activity before breakdown. Therefore, there may be assumed that for the cylindrical symmetrical Config. 2, partial discharge activity decreases with increasing average background field. The correlation where a smaller background field results in increased number of periods with observed activity is not observed in Figure 15a.

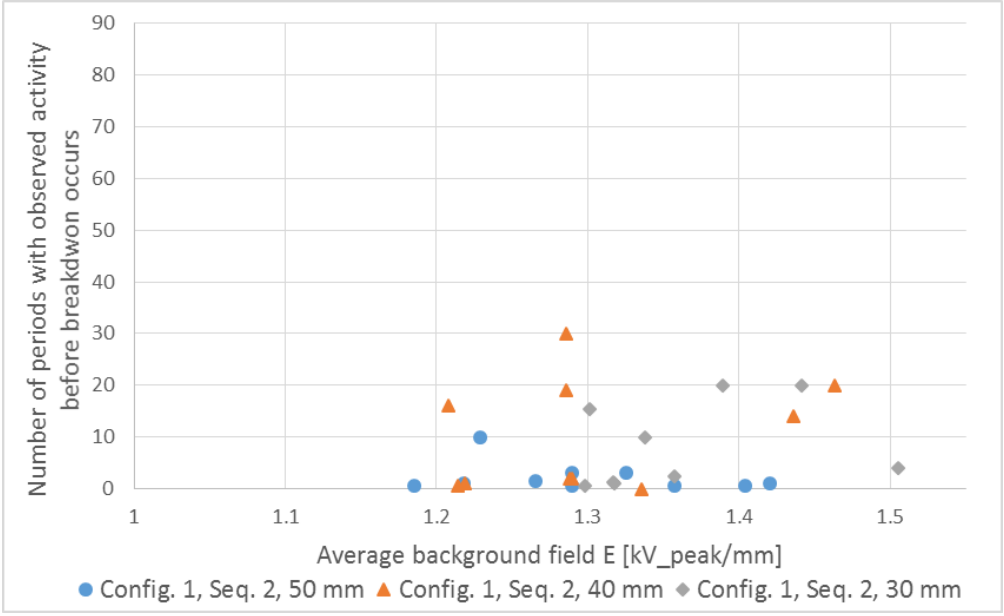

(a) Config. 1. Number of points for 50 mm equals 11 (circle), number of points for 40 mm equals 10 (triangle), and number of points for 30 mm equals 9 (diamond).

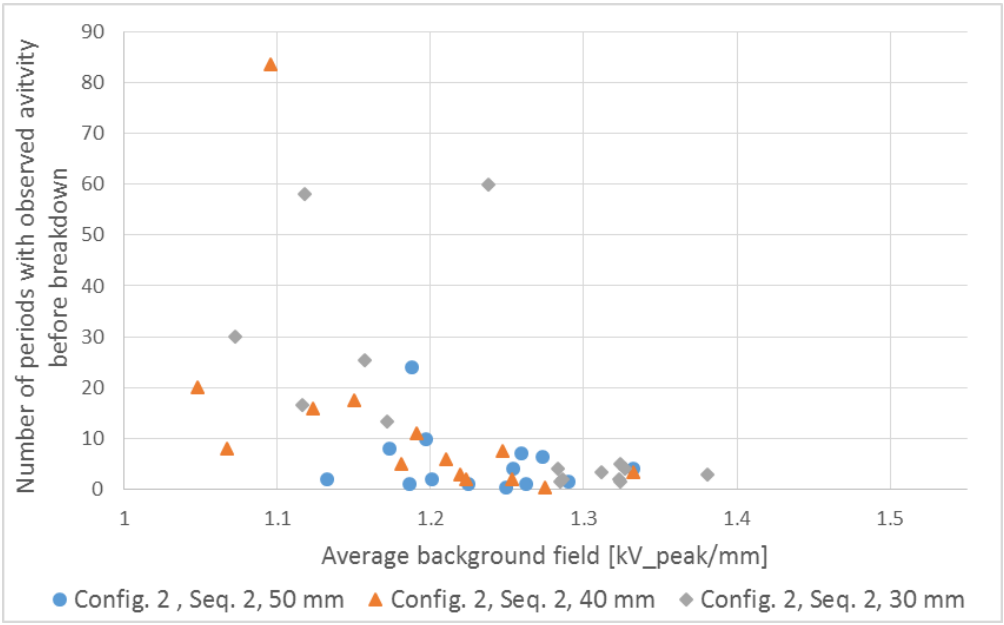

(b) Config. 2. Number of points for 50 mm equals 14 (circle). The number of points for 40 mm (triangle) and 30 mm (diamond) equals 15.

Figure 15: Visually estimated number of periods with partial discharge activity before breakdown. Circle represent gap distance $d = 50$ mm, triangle represent $d = 40$ mm and diamond represent $d = 30$ mm.

4.3 Simulations

The following section presents the results from simulations performed in COMSOL Multiphysics. As mentioned in Section 3.3, the simulations are computed with a gap distance of 50mm and $U = 100\,\text{kV}$ for easily comparison of the simulations.

The following results are presented:

- Surface plot of electric field strength and streamlines for calculation of inception voltage are shown in Figure 16.
- Normal components of the electric field along streamlines as a function of arc length are seen in Figure 17.
- The inception voltages, calculated by integrating eq. (2) along the streamlines shown in Figure 16, are presented in Table 3.

Figure 16 shows surface plots of electric field strength. Note that the subfigures have an approximately equal maximum value on the color legend. Figures 16c and 16d show enlarged images of the upper electrode. The coloured regions in these subfigures show the areas where $E > 2.5\,\text{kV/mm}$, i.e. the predicted area for streamer inception. Streamline 1 for both configurations start in the point of maximum field on the edge near the triple junction. According to Section 2.2.1, the integration path for calculating the streamer inception criterion, given by eq. (2), starts at the point with maximum field strength and follows the field line provided that $\alpha_{eff}(E) > 0$. For Config. 1, streamline 3 starts in the point of maximum field on the sharp edge, shown in Figure 7b.

Due to the fact that streamers do not penetrate the rod, streamline 2 is defined from the mesh coordinate where streamline 1 penetrates into the rod domain.

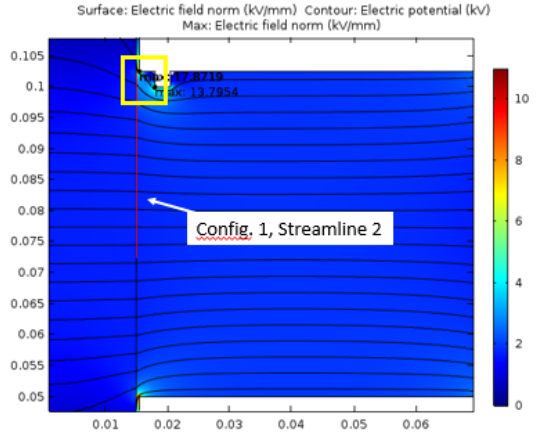

(a) Config. 1. The black curves are the equipotential lines. The red line along the rod shows Config. 1, streamline 2, used for calculation of the inception voltage. The rectangle on the upper electrode shows the area in 16c.

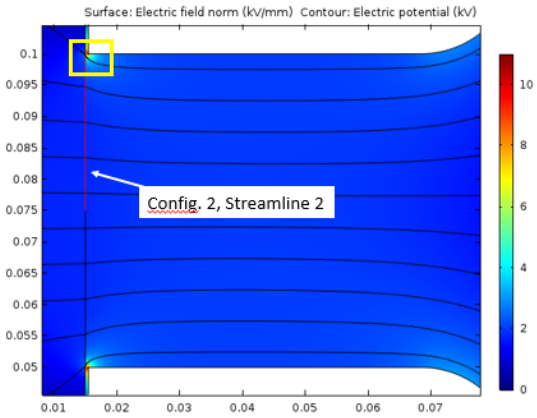

(b) Config. 2. The black curves are the equipotential lines. The red line along the rod shows Config. 2, streamline 2, used for calculation of the inception voltage. The rectangle on the upper electrode shows the area in 16d.

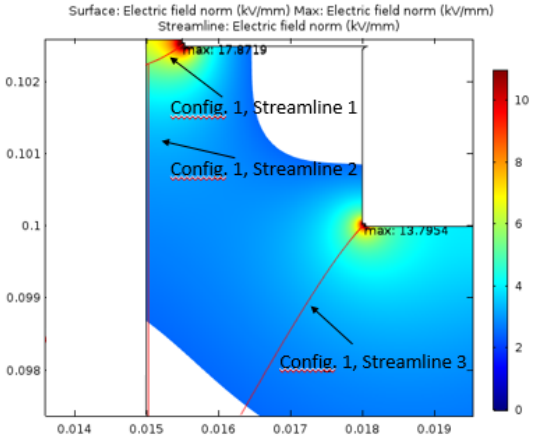

(c) Config. 1. Enlarged image of the upper electrode. The coloured region in the air domain shows the area where $E > 2.5\,\mathrm{kV/mm}$. Streamlines for evaluation of normal component of electric field are marked with red lines. Streamline 1 starts in the point of maximum field on the edges of triple junction, and Streamline 3 starts in the point of maximum field on the sharp edge with geometry shown in Figure 7b.

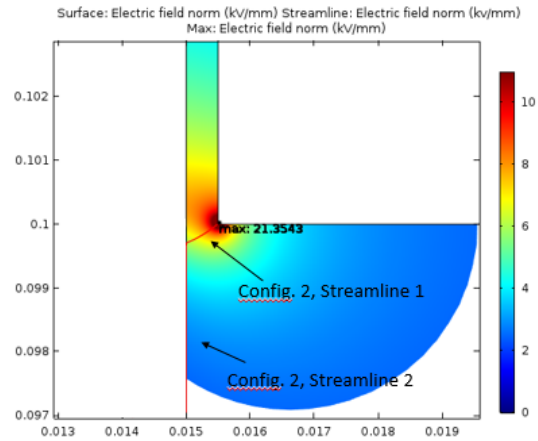

(d) Config. 2. $U_{peak} = 56.2\,\mathrm{kV}$. Enlarged image of the upper electrode. The coloured region shows the area where $E > 2.5\,\mathrm{kV/mm}$. Streamlines for evaluation of normal component of electric field are marked with red lines. Streamline 1 starts in the point of maximum field on the edge of triple junction.

Figure 16: Surface plot of electric field strength. $U_{peak} = 100\,\mathrm{kV}$ and $d = 50$ mm for both configurations.

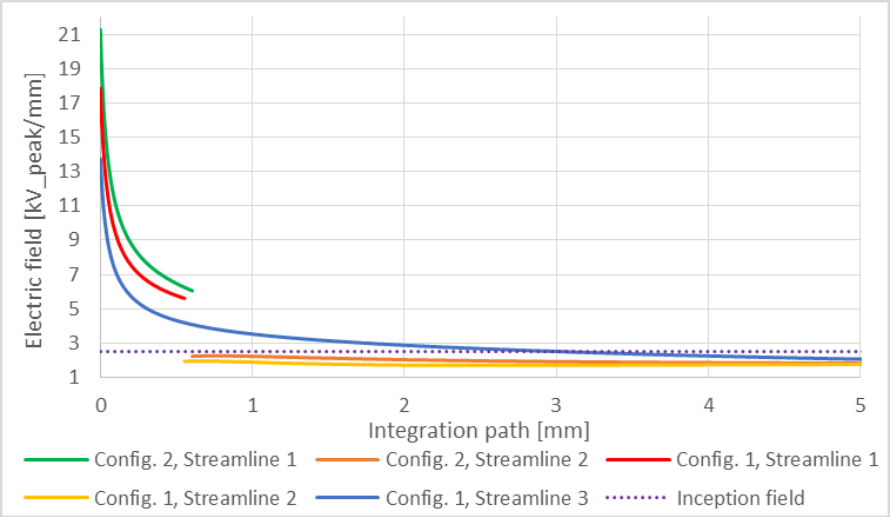

Figure 17: Electric background field (vertical axis) as a function of the integration path (horizontal axis) along streamlines shown in Figure 16. The green line (Config 1, Streamline 1), red line (Config. 2, Streamline 1), and blue line (Config. 1, Streamline 3) show the normal component of the background field as a function of the arc length along the streamlines. The yellow (Config. 1, Streamline 2) and orange line (Config. 2, Streamline 2) shows the z-component of the background field along the rod, i.e. the z-component in Figure 6. The dotted line is the limit where $E = 2.5\,\mathrm{kV/mm}$, where, according to Section 2.2.1, $\alpha_{eff}(E) = 0$.

Figure 17 shows the electric background field (vertical axis) as a function of the integration path (horizontal axis) along streamlines shown in Figures 16c and 16d. The green line (Config 1, Streamline 1), red line (Config. 2, Streamline 1) and blue line (Config. 1, Streamline 3) show the normal component of the background field as a function of the arc length along the streamlines. The yellow (Config. 1, Streamline 2) and orange line (Config. 2, Streamline 2) show the z-component of the background field along the rod, i.e. the z-component in Figure 6. The dotted line shows the limit where $E = 2.5\,\mathrm{kV/mm}$, where, according to Section 2.2.1, $\alpha_{eff}(E) = 0$, and integration path in eq. (2) stops.

It is seen from the yellow and orange line that the z-component of the background field along the rod has a value lower than the limit for inception, $E = 2.5\,\mathrm{kV/mm}$, and that the integration path in eq. (2) stops when the streamline 1 penetrates the rod.

Table 3: Inception voltage, calculated by integrating eq. (2) along the streamlines shown in Figure 16.

	$\mathbf{U}_i$ [kV_{peak}]
Config.1, Streamline 1 and 2	84.0
Config.1, Streamline 3	101.2
Config.2, Streamline 1 and 2	71.2

Table 3 shows the inception voltage, calculated by integration of eq. (2) along the presented streamlines, with $\alpha_{eff}(E)$ as given in Appendix A.1. The table shows that Config. 1 has a higher inception voltage than Config. 2 for the streamline starting at the triple junction.

Furthermore, the calculated inception voltage for Config. 1, Streamline 3, is 20% higher than Config. 1, Streamline 2, and streamers are assumed not to be incepted in the point of local maximum field at the sharp edge. This is substantiated that the fact that the maximum electric field is higher at the triple junction than at the sharp edge, as seen in **??**.

4.4 Comparison of Measured Voltages and Simulations

It is chosen to compare the inception voltage, shown in Table 3, for the streamlines starting in the triple junction, with the measured voltages for the equal gap distance, i.e. $d = 50$ mm.

Table 4 shows the average breakdown voltage, 99 % minimum value, calculated

Table 4: Average breakdown voltages, 99 % minimum value, calculated inception voltages, and the percent difference between measured voltages and calculated voltages.

	$\mathbf{U}_{50}$ [kV_{peak}]	$\mathbf{U}_{min.\ 99\%}$ [kV_{peak}]	$\mathbf{U}_i$ [kV_{peak}]	**% diff. $\mathbf{U}_{50}$ and $\mathbf{U}_i$**	**% diff. $\mathbf{U}_{min.\ 99\%}$ and $\mathbf{U}_i$**
Config.1 Streamline 1,2	74.6	54.0	84.0	12.6	55.6
Config. 2 Streamline 1,2	61.1	53.7	71.2	16.5	32.6

inception voltages, with integration path along streamlines 1 and 2, and the

percent difference between measured breakdown voltages and calculated inceptions voltages.

The table shows that there is a difference of 12.6% between average breakdown voltage and calculated inception voltage for Config. 1, and furthermore a difference of 55.6% between the 99 % minimum value and calculated inception voltage. Moreover, the difference between average breakdown voltage and calculated inception voltage for Config. 2 is 16.5% and the difference between the 99 % minimum value and calculated inception voltage is 32.6%.

The calculated inception voltage is higher than the measured average breakdown voltage. This may be due to the fact that the simulation model, and furthermore the equations in Appendix A.1 applied for calculating eq. (2), do not consider the charge transfer that, according to Section 2.4, occurs when materials of different nature are put into contact, which is the case for triple junctions. Moreover, Section 2.4 predicts that high field concentrations at the triple junction might set up a cathode mechanism which encourages the initiation of discharges, and in addition, charges deposited on the surface by corona might alter the electric field distribution, encouraging breakdown.

5 Conclusions

The following conclusions can be drawn:

- The investigated test objects have a higher withstand voltage than the withstand voltage for streamer propagation.
- The deviation between the measured withstand voltage and the withstand voltage for streamer propagation increases with increasing gap distance. The withstand voltages for the investigated test objects and gap distances are located in area of streamer inception, i.e. to the left of point P in Figure 1. Ergo: The streamer inception criteria, given by eq. (2), should be the dimensioning criteria for the the withstand voltage of the investigated test objects at the examined gap distances.
- All measurements indicate that the largest amount of optically detected discharges align with the commonly observed phase-resolved pattern for gliding discharges along a surface of a solid dielectric in air.
- When partial discharge activity is detected, breakdown occurs within predominantly 30 periods. Therefore: When an AC stress is applied, charges deposited on the surface is predicted to influence the discharge activity in the consecutive period, and the time aspect of the applied voltage must be taken into account.
- The calculations of the inception voltage based on starting in the point of maximum field and following the streamline for the background field gives an inception voltage that is higher then the measured withstand voltage. Therefore: streamer inception criterion based on applying the background field for the equations in Appendix A.1 results in a dimensioning criteria where the withstand voltage is lower than the dimensioning inception voltage from calculations.
- Inception voltage should be the dimensioning criteria for the investigated test objects. However, it is predicted that the charge transfer between the materials at the triple junctions should be considered when formulating the dimensioning criteria for streamer inception at triple junctions.

6 Further Work

For further work, following are proposed:

- For further examination of the investigated test objects it would be appropriate using two photomultiplier tubes for accessing the area on the rear of the rod.
- The observation of surface charges must be investigated further.
- Examine a test object only consisting of the high voltage part of the investigated configurations in this work. The idea is that breakdown is avoided, and this simplifies the task by detecting activity at voltage levels close to inception voltage. When breakdown is avoided, electric measurement of partial discharge activity may be considered as a supplement to optical detection.
- Using a camera for detecting the location and development of discharges and propagation of avalanche and investigating activity around triple junction.
- Designing a rig where only the test object and the PMT are covered by curtains for easier assess to the test cell.

7 References

[1] Ilstad, E. (2014) *TET 4160 High VOltage Insulation Materials*, NTNU, Department of Electric Power Engineering, Trondheim

[2] United Nations, Framework Convention on Climate Change *Global Warming Potentials*, (2014) Available:`http://unfccc.int/ghg_data/items/3825.php` (10.12.2015)

[3] Stocker, T.F., D. Qin, G.-K. Plattner, M. Tignor, S.K. Allen, J. Boschung, A. Nauels, Y. Xia, V. Bex and P.M. Midgley (eds.) *Climate Change 2013: The Physical Science Basis*, Available:`http://www.climatechange2013.org/images/report/WG1AR5_Chapter08_FINAL.pdf` (01.03.2016)

[4] Statens forurensningstilsyn (2011). *Reduksjon i utslippene av HFK, PFK og SF6*, Available: `http://www.miljodirektoratet.no/old/klif/publikasjoner/luft/1754/ta1754.pdf` (11.09.2015)

[5] Goldman, A. Goldman, M. Odic, E. Dessante, Ph. (2008). Partial discharges inception and ageing effects in a gas insulated HV equipment *Gas Discharges and Their Applications, 2008. GD 2008. 17th International Conference on*(pp. 49-56) Cardiff: IEEE

[6] Blaszczyk, A. Böehme, H. Christen, T. Pedersen, A. (2009). Streamer inception and propagation models for designing air insulated power devices *Electrical Insulation and Dielectric Phenomena, 2009. CEIDP '09. IEEE Conference on* (pp. 604-607). Virginia Beach, VA: IEEE

[7] Blaszczyk, A. Böehme, H. Christen, T. Pedersen, A. (2011). Streamer Line Modelling. B. Michielsen, J-R. Poirier (Eds.), *Scientific Computing in Electrical Engineering SCEE 2010*(pp. 173-181). Berlin: Springer Berlin Heidelberg.

[8] Lemke, E. el. al. (2008). Guide for Partial Discharge measurement in compliance to IEC 60270 *Working group D1.33* Cigré

[9] F.H.Kreuger (1992). Industrial High Voltage *Vol. II* Delft: Delft university Press

[10] Schwarz, R. Muhr, M. (2007). Modern Technologies in Optical Partial Discharge Detection *Electrical Insulation and Dielectric Phenomena, 2007. CEIDP 2007. Annual Report - Conference on* (pp. 163-166). Vancouver, BC: IEEE

[11] Yang, X. Ming, Y. Xiaolong, C. Changrong, Q. Chen, G. (2000). Comparison between Optical and Electrical Methods for Partial Discharge Measurement

Properties and Applications of Dielectric Materials, 2000. Proceedings of the 6th International Conference on (pp. 300-303 vol.1) Xi'an: IEEE

[12] Allan D.J. et. al. (1996). High voltage engineering and testing *IEE Power Seried 17, Peter Peregrinus Ltd. on behalf of the Institution of Electrical Engineers*. London: Peter Peregrinus Ltd. on behalf of the Institution of Electrical Engineers, London, United Kingdom

[13] Cactus 2000. *Air humidity calculation,* Availible: `http://www.cactus2000.de/js/calchum.pdf` (13.04.2016)

[14] Støa-Aanensen, N. *SINTEF Energy Research Project Memo, AN15.14.63 - Initial AC breakdown testing*

[15] Korneliussen, K. (2015) *Streamer propagation along insulator surface under AC stress*. Department of Electric Power Engineering, Trondheim

[16] Goldman, A. Goldman, M. Odic, E. Dessante, Ph. (2008). *OSC BRUKSANVISNING*(pp. 49-56) Cardiff: IEEE

[17] *PHOTOMULTIPLIER TUBES, Basics and Applications, THIRD EDITION (Edition 3a)* (2007) HAMAMATSU PHOTONICS K. K.

[18] Photomultiplier Tubes. Construction and Operating Characteristics. Connections to External Circuits Available: `https://wwwmu.mpp.mpg.de/docs/pmtconstruct.pdf` (18.02.2016)

[19] *Hamamatsu Product Bulletion PB-103-01* (1982) Hamamatsu TV Co., Ltd

[20] Zaengl, W. S. Petcharaks, K. (1994). Applicability of the streamer breakdown criterion to inhomogeneous gas gaps. L. G. Christophorou, D. R. James (Eds.), *Gaseous Dielectrics VII*(pp. 153-159). United States: Springer US.

A Appendix

A.1 Equations for calcuating Inception Voltage

For synthetic air where $2.588 < E/p < 7.943$ kV/mm $\cdot$ bar, $\alpha_{eff}(E)$ can be calculated using [20]:

$$\frac{\alpha_{eff}}{p} = 1.6053 \left[\frac{E}{p} - 2.165\right]^2 - 0.2873, \tag{12}$$

where E is the background electric field, and the pressure p, is normalized for 20°C. Note that eq. (12) is essentially eq. (2) generalized with a field dependent α along curved trajectories.

When $7.943 < E/p < 14$ kV/mm $\cdot$ bar, $\alpha_{eff}(E)$ can be calculated using [20]:

$$\frac{\alpha_{eff}}{p} = 16.7766 \frac{E}{p} - 80.0006. \tag{13}$$

A.2 Measurement Results

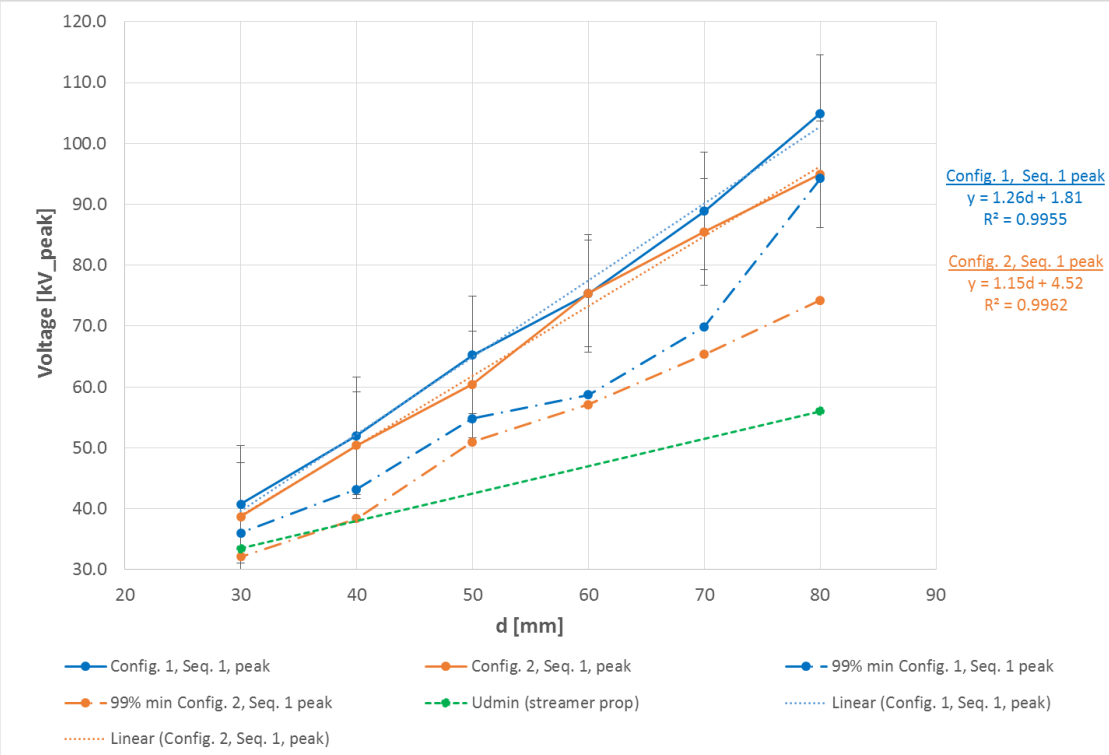

Figure 18: Average breakdown voltage (vertical axis) as a function of gap distance (horizontal axis); linear polynomials, standard error (SE), and 99 % minimum confidence values for Seq. 1. The blue points and lines represent Config. 1, and the orange points and lines represent Config. 2. The green line illustrates eq. (3) with associated parameters for AC stress.

A.3 MATLAB: Calculation of number of electrons

Table 5: Noise limits

Config.	**Limit** [mV]	**Break loop if**	break limit [mV]	files maniplated
Config. 1, Seq. 2, 50 mm	−20	25	−10	NO
Config. 1, Seq. 2, 40 mm	−25	25	−5	NO
Config. 1, Seq. 2, 30 mm	−25	25	−5	NO
Config. 2, Seq. 2, 50 mm	−25	10	−5	YES
Config. 2, Seq. 2, 40 mm	−25	10	−5	YES
Config. 2, Seq. 2, 30 mm	−25	10	−5	YES

```
%This script read an ASCII file into a matrix and search the matrix for
%values of pd lower than an certain value. If the pdvalue is lower, the
%counter in Vmatrix is updated for that given angle.

pdvalue=-25E-3;
pdEdge = 10; %if #pdEdge is observed after each other, file breaks.
pdEdgevalue = -5E-3;
f= 50; % frequency in hz
T_tot=20E-3*10; %ms per div * num. div (10)
omega=2*pi*f;
deltaThetaTOT=pi/64; %radian , 5.62 degree pi/32 or 2.8125 degree pi/64 rad
Vmatrix(:,1)=(0:deltaThetaTOT:2*pi); %[rad]
xax=Vmatrix(:,1); %For plotting
Vmatrix(:,2)=zeros;
amplitude = 300;
y=amplitude*cos(xax); %For plotting waveform
Vtemp(:,1) = zeros;%saving angles
angleTemp=0;
```

```
output_name = 0;
output_i = 0;
output_V = 0;
output_angle = 0;

filename = cellstr(ls('*.csv'));
delimiterIn = ',';
headerlinesIn = 15; %Fifteen rows with including text.
for k = 1:length(filename) %!!!!!!!!
A = importdata(filename{k},delimiterIn,headerlinesIn);
Mtemp=A.data;
%%%%%%%%%%%%%%%%%%%%%%%%%%%%%%%%%%%%%%%%%%%%%%
numofsample=length(Mtemp);
V_trig=Mtemp(1,3);
deltaT=T_tot/numofsample; %[seconds].
deltaTheta=omega*deltaT; %radian
Vmax = max(Mtemp(:,3));
%theta0=pi + acos(V_trig/Vmax); %if negavtive trig, negative slope
theta0=2*pi - acos(V_trig/Vmax); %if positive trig rising slope
%acos(V_trig/Vmax) gives two angles.

n=0;
i=1;
theta=0;
count=0;
temp = 0;
countpd=0;
lastrowpd=Mtemp(1,2);
pdcounter= false;
q=0; %placeholder in Vtemp
pdyesno=0;

for i=1:numofsample
    pd=Mtemp(i,2);
    if pd<pdvalue
        Mtemp(i,1)=1;
    else
        Mtemp(i,1)=0;
    end
    temp=(i-1)*deltaTheta + theta0;
    theta = mod(temp,2*pi);
    Mtemp(i,4)=theta;
    Mtemp(i,5)=i*deltaT-deltaT;

    pdyesno=Mtemp(i,1);
    if pdyesno ==1 %if the value in col. 1, row i, is lower than pdvalue.
        rowTemp=Mtemp(i,4); %retrieves angle where value on pd < pdvalue
```

```
    q=q+1;
    Vtemp(q,1)=rowTemp;   %storing the angle hver pd is observed
end
if i>1
lastrowpd=Mtemp(i-1,2);
   if lastrowpd<pdEdgevalue;
      countpd=countpd+1;
      if countpd == pdEdge
         pdcounter = true;
      end
   else
        countpd=0;
   end
end
count=0;

if pdcounter
    lengthVtemp=length(Vtemp)-pdEdge;
    for m=1:lengthVtemp %plotting pd referred to angle.
        angleTemp=Vtemp(m);
        for j=1:(length(Vmatrix)-1)
        rowLow=Vmatrix(j,1);
        rowHigh=Vmatrix(j+1,1);
            if(rowLow<=angleTemp) && (rowHigh>angleTemp)
                count=Vmatrix(j,2);
                count=count+1;
                Vmatrix(j,2)=count;
            end
        end
    end

    output_name = filename{k};
    output_i= i;
    fprintf(' Name of file: %s\n',output_name)
    fprintf(' Ending at row: %d\n',output_i)
            figure('name',output_name,'NumberTitle','off')%for control plot
            plot(Mtemp(1:i-pdEdge,1),'b')
            hold on
            plot(Mtemp(1:length(Mtemp),2),'r')
            axis([0 inf -1 1.05])
    break

else if i==numofsample
        lengthVtemp=length(Vtemp)-pdEdge;
    for m=1:lengthVtemp %plotting pd referred to angle.
        angleTemp=Vtemp(m);
        for j=1:(length(Vmatrix)-1)
        rowLow=Vmatrix(j,1);
        rowHigh=Vmatrix(j+1,1);
```

```
                if(rowLow<=angleTemp) && (rowHigh>angleTemp)
                    count=Vmatrix(j,2);
                    count=count+1;
                    Vmatrix(j,2)=count;
                end
            end
        end
        end
    end
end
end

%plot of number of observed pds at certain angels
figure('name','SFC_30mm_matlab','NumberTitle','off') %for control plot
h(1)=bar(Vmatrix(:,1),Vmatrix(:,2));
set(gca,'xlim',[-2*pi() 2*pi()],'xtick',-2*pi():pi()/2:2*pi(),'xticklabel',{'-2p' '-3
xlabel('Phase [rad]','fontname','helvetica','fontsize',10)
ylabel('Num. of pd','fontname','helvetica','fontsize',10)
hold on;
%plot of cosine as a visual reference to the number of observed pds
h(2)=plot(xax,y);
xlim([0 2*pi])

saveas(gcf,'SFC_30mm_matlab_25_value', 'png') %save to file
```